Multiple-stage deglacial retreat of the southern Greenland Ice Sheet linked with Irminger current warm water transport

Paul Knutz, Marie-Alexandrine Sicre, Hanne Ebbesen, Sarah Christiansen, Antoon Kuijpers

Multiple-stage deglacial retreat of the southern Greenland Ice Sheet linked with Irminger Current warm water transport

Paul C. Knutz,[1] Marie-Alexandrine Sicre,[2] Hanne Ebbesen,[1] Sarah Christiansen,[3] and Antoon Kuijpers[1]

Received 10 September 2010; revised 4 March 2011; accepted 3 May 2011; published 30 July 2011.

[1] There is limited knowledge pertaining to the history of the Greenland Ice Sheet (GIS) during the last glacial-interglacial transition as it retreated from the continental margins to an inland position. Here we use multiproxy data, including ice-rafted debris (IRD); planktonic isotopes; alkenone temperatures; and tephra geochemistry from the northern Labrador Sea, off southwest Greenland, to investigate the deglacial response of the GIS and evaluate its implications for the North Atlantic deglacial development. The results imply that the southern GIS retreated in three successive stages: (1) early deglaciation of the East Greenland margins, by tephra-rich IRD that embrace Heinrich Event 1; (2) progressive retreat during Allerød culminating in major meltwater releases (δ^{18}O depletion of 1.2‰) at the Allerød–Younger Dryas transition (12.8–13.0 kyr B.P.); and (3) a final stage of glacial recession during the early Holocene (~9–11 kyr B.P.). Rather than indicating local temperatures of ambient surface water, the alkenones likely were transported to the core site by the Irminger Current. We attribute the timing of GIS retreat to the incursion of warm intermediate waters along the base of grounded glaciers and below floating ice shelves on the continental margin. The results lend support to the view that GIS meltwater presented a forcing factor for the Younger Dryas cooling.

Citation: Knutz, P. C., M.-A. Sicre, H. Ebbesen, S. Christiansen, and A. Kuijpers (2011), Multiple-stage deglacial retreat of the southern Greenland Ice Sheet linked with Irminger Current warm water transport, *Paleoceanography*, *26*, PA3204, doi:10.1029/2010PA002053.

1. Introduction

[2] The northwest Atlantic is an important junction in the global ocean-climate system due to major water mass conversion taking place in proximity to the southern Greenland Ice Sheet (GIS). Presently, cooling of surface waters within the subpolar gyre generates Labrador Sea Water that forms a major intermediate contribution to Atlantic Meridional Ocean Circulation (AMOC) [*Talley and McCartney*, 1982; *Cheng and Rhines*, 2004].

[3] The last deglaciation (~1–19 kyr B.P.) was commensurate with a northward migration of the polar front and advection of temperate water masses via the Irminger Current into the Labrador Sea and along the west coast of Greenland [*Hillaire-Marcel et al.*, 1994; *Rahman and de Vernal*, 1994]. This long-term climate amelioration was interrupted by periods of coolings (stadials), widely recognized in marine and ice core records [*Bond et al.*, 1993; *Dansgaard et al.*, 1993] as Heinrich Event 1 (HE 1: 16–17 kyr) and the Younger Dryas cold reversal (11.6–12.8 kyr). The stadials are commonly associated with meltwater and iceberg discharges capable of AMOC perturbations resulting in globally significant ocean reorganizations [*Broecker et al.*, 1990; *Zahn et al.*, 1997; *Hughen et al.*, 1998]. Heinrich events, identified by pronounced increases in carbonate-rich IRD that reoccur at ~7 kyr intervals, are attributed to iceberg armadas from the Laurentide Ice Sheet (LIS) through the Hudson Strait [*Andrews and Tedesco*, 1992; *Hemming*, 2004]. Cores collected from the east Greenland margin and the adjacent basins display IRD cycles that, in terms of frequency, resemble the atmospheric Dansgaard-Oeschger (D-O) oscillations [*Nam et al.*, 1995; *Stein et al.*, 1996; *Hagen and Hald*, 2002]. High-resolution studies, advocating a more implicit role of the GIS in past climate change, suggests that Greenland meltwater emissions may have been crucial for limiting deep water formation during stadials [*van Kreveld et al.*, 2000] and could be responsible for the Younger Dryas cooling [*Jennings et al.*, 2006].

[4] During the last glacial to interglacial transition the GIS retreated from its glacial maximum limit, probably at or near the shelf edge, to its present land-based configuration [*Dowdeswell et al.*, 1998; *Bennike and Björck*, 2002; *Funder et al.*, 2004; *Simpson et al.*, 2009]. Cosmogenic isotope and radiocarbon dating of till, lake and glacial-marine deposits suggest that ice withdrew from the continental margins south of 72°N in several discrete phases between 8 and

[1]Geological Survey of Denmark and Greenland, Copenhagen, Denmark.
[2]Laboratoire des Sciences du Climat et de l'Environnement, IPSL, CNRS/CEA/UVSQ, Gif-sur-Yvette, France.
[3]Institute for Geography and Geology, University of Copenhagen, Copenhagen, Denmark.

0883-8305/11/2010PA002053

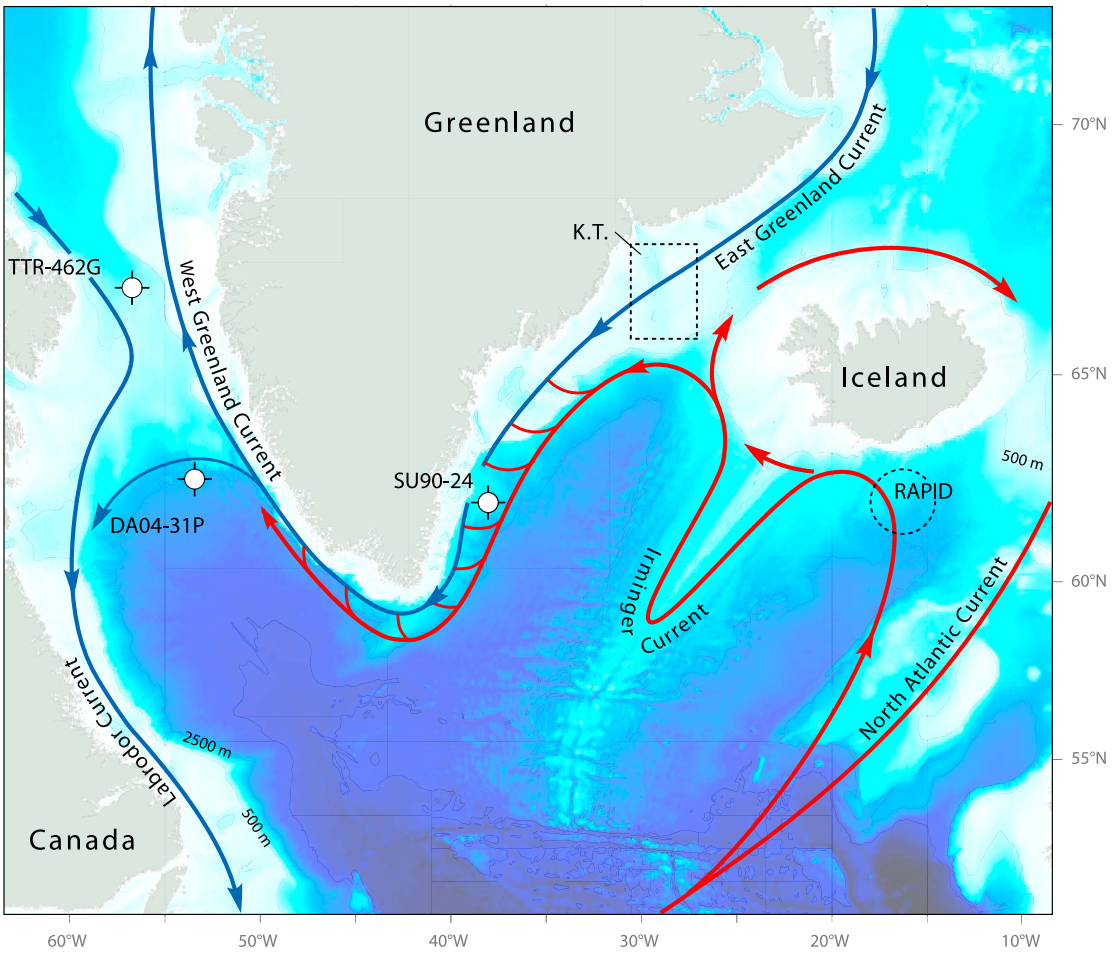

Figure 1. Map of northwest Atlantic displaying cold and warm surface currents, the position of core DA04-31P, and other sites referred to in the text. K.T. is the Kangerlussuaq Trough.

15 kyr [*Funder and Hansen*, 1996; *Bennike et al.*, 2002; *Long et al.*, 2008; *Rinterknecht et al.*, 2009; *Roberts et al.*, 2009]. A key question relates to the response time of the GIS to interhemispheric climate forcing, which for the last glacial-interglacial transition has prompted diverse opinions [*Bennike and Björck*, 2002; *Carlson et al.*, 2008a]. In this paper we apply multiproxy paleoceanographic data from the continental margin off southwest Greenland to elucidate the late glacial to early Holocene history of the GIS in the context of regional oceanographic changes.

[5] The mechanisms responsible for the disintegration of the Pleistocene ice sheets has yet to be fully understood but several hypotheses have been proposed: (1) Internal ice sheet oscillations or binge/purge model [*MacAyeal*, 1993], (2) collapse of fringing ice shelves [*Hulbe et al.*, 2004] (3) jökulhlaups representing catastrophic bursts of ice dammed lakes [*Johnson and Lauritzen*, 1995] and (4) sea level rises resulting from halted ocean circulation [*Flückiger et al.*, 2006]. Except for (1), some form of climate-related forcing is required to destabilize glacial margins and induce massive iceberg fluxes as seen during Heinrich Events. This has stimulated detailed studies focusing on relationships between climate, ocean circulation changes and glacial collapses in the North Atlantic region e.g., [*Lagerklint and Wright*, 1999; *Knutz et al.*, 2002; *Moros et al.*, 2002]. In terms of the GIS, *Alley et al.* [2010] emphasize its sensitivity to temperature forcing (induced by atmospheric or oceanic propagation), resulting in growth phases during cold periods and shrinkage during periods of climate warming. Here we combine analyses of ice-rafted components and marine environmental indicators at centennial-scale resolution to address mechanisms of ice sheet/ocean interactions during last deglaciation. In the discussion, we focus on the role of ocean heat transport as a factor for GIS variability and, by implication, the Younger Dryas cooling.

2. Oceanographic Setting

[6] The surface hydrography of the Labrador Sea is influenced by the transport of cold and low-saline water masses ($\theta \sim -1.8$°C, S $\leq$ 34.5‰) southward from the Arctic Ocean, along the Greenland shelf margins (Figure 1) [*McCartney and Talley*, 1982; *Cuny et al.*, 2002]. The East Greenland Current forms a hydrographic and thermal barrier that isolates the Greenland coastal glaciers from warm Irminger Sea Water (ISW: $\theta \sim 4.5$°C, S $\leq$ 35‰) transported by the Irminger

Table 1. Information on AMS ^{14}C Dates Obtained From Core DA04-31P

Core/Depth (cm)	Laboratory Number	Material	^{14}C Ages ± 1σ (years B.P.)	MR Age[a] (years B.P.)	Calibrated 2σ Age Ranges (years B.P.)	Calibrated Age (years B.P.)
3–6	AAR-10681	Nps	1365 ± 40	400	944–1158	1040
38	AAR-9982	Nps	8420 ± 65	400	8841–9246	9010
44–46	AAR-10458	Nps	8440 ± 55	400	8925–9247	9050
66	AAR-10682	Nps	8270 ± 47*	n/a		
94–98	AAR-10703	Nps	11080 ± 65	600	10225–12586	12,430
122	AAR-10820	Nps	12710 ± 160	600	13,583–14,646	13,970
150	AAR-10683	Nps	13,020 ± 65	600	14,112–14,984	14,420
156	AAR-9984	Nps	21,880 ± 170*	n/a		
206	AAR-9985	Nps	14,660 ± 90	1000	16,548–17,020	16800
292	AAR-10684	Nps	16,670 ± 100	600	18,914–19,430	19,260
634	AAR-9986	Nps	22,320 ± 170	400	25,821–26,894	26,240
743	AAR-10685	Nps	26,550 ± 250	400	30,417–31,179	30,930

[a]Correction estimates for marine reservoir age beyond the modern value of 400 years [*Bard et al.*, 1998] are based on *Waelbroeck et al.* [2001], *Bondevik et al.* [2006], and *Franke et al.* [2008]. Asterisks denote ages representing stratigraphic inversions. Calibrated ages used for the age model (Figure 2) either represent the modal peak or, in the case of double peaks, the mean value of the 1σ range.

Current. The core of this water mass is distinguishable by its properties, vertically down to 700 m and horizontally landward of the 3000 m isobath. As the East Greenland Current reaches the southern tip of Greenland it mixes with subsurface ISW, and as a result becomes more saline (34.4–35.5‰) and warmer with seasonal surface temperatures between 3°–8°C. This water mass propagates northward in form of the West Greenland Current that semicirculates the northern Baffin Bay while incorporating arctic surface waters from the Nares Strait and the Canadian Arctic Archipelago. The resulting Baffinland Current continues southward and upon crossing the Davis Strait, it merges with a crossover branch of the West Greenland Current to form the Labrador Current. Because of this exchange between Irminger Sea Water and Arctic surface waters, surface salinities and temperatures on the Labrador Shelf are several degrees lower than along the southwest Greenland margin.

[7] Labrador Sea Water (LSW) is formed by open-ocean convection in the subpolar gyre during winter months [*Talley and McCartney*, 1982; *Dickson and Brown*, 1994] and occupies intermediate depths of the Labrador basin, between 800–1500 m. LSW imparts a middepth stratification in the Labrador Sea basin beyond which it spreads laterally into the North Atlantic water mass structure under the influence of anticyclonic lateral mixing [*Lavender et al.*, 2000]. A portion of LSW is entrained into the Deep Western Boundary Undercurrent (DWBU) that transports North Atlantic Deep Water south along the North American continent. In the Labrador Sea basin, the DWBU displays a strong, barotropic current with a main core flowing above the lower continental slope close to the 3000 m isobath [*Cuny et al.*, 2002].

3. Sample Material and Methods

[8] Piston core DA04-31P (62 33.78 N, 54.22 W; water depth 2525 m, length 8.78 m) was retrieved by R/V *Dana* in 2004. The coring target was an area of muddy drift sedimentation on a gentle section of the slope, above the main trajectory of the DWBU (Figure 1).

[9] Multielement geochemical data were measured at 1 cm resolution on split core sections using the Avaatech XRF facility at NIOZ. Tube voltages of 10 and 30 kV and 50 kV (Ba) were applied. The same sections were color scanned and measured for gamma ray (GR) density using a GEOTEK multisensor logger. The calcium carbonate content was determined on 7 samples by HCl stoichiometric titration in order to provide a quantitative calibration for XRF Ca.

[10] The upper 235 cm of core DA04-31P, corresponding to the late glacial to Holocene interval was sampled at 1–2 cm intervals. The petrology of ice-rafted debris (IRD) components and volcanic tephra was determined by visual microscopic inspection of the >250 μm fraction. Apart from assisting grain identification this threshold favors an origin from melting icebergs, as opposed to other transport processes [*Andrews et al.*, 1997]. Sieved samples were split into subfractions containing a minimum of 400 grains. The abundance of detrital components is reported as number of grains per gram dry sediment.

[11] The total abundance of planktonic foraminifer and the species abundance of *Neogloboquadrina pachyderma* sinistral (Nps) was determined. The content of diatoms in the 125–250 μm fraction was semiquantified on a 1–5 scale with following denotation: 1 = absent, 2 = rare, 3 = noticeable presence, 4 = abundant, 5 = high abundance. Oxygen isotope measurements, performed on batches of 30–40 specimens of Nps picked from the >250 μm fraction, were carried out at Woods Hole Oceanographic Institution using a Finnigan MAT252 mass spectrometer with a Kiel carbonate device. Values were calibrated against internal standards and converted to the Vienna PDB scale. The recorded analytical reproducibility was routinely better than ±0.06‰ (±1σ).

[12] The quantity and depth position of samples for AMS ^{14}C analyses was partly determined by the generally sparse but variable presence of planktonic foraminifers (Table 1); 700–1000 mg of Nps shells were picked from the >250 μm fraction and analyzed at Aarhus University Radiocarbon Laboratory. Holocene and pre-LGM dates were corrected for the marine reservoir (MR) effect by subtracting 400 years, equivalent to the modern age of subsurface North Atlantic waters [*Bard et al.*, 1998; *Lloyd et al.*, 2005]. For dating samples representing the glacial to interglacial transition (LGM to Younger Dryas) a MR age of 600 years was applied, following *Bondevik et al.* [2006] and *Franke et al.* [2008]. For the single date corresponding to the base of the HE 1

event, an MR age of 1000 years was assumed due to a strong meltwater effect implied by previous studies [*Waelbroeck et al.*, 2001]. It is noted that these MR estimates involve a large degree of uncertainty, on the scale of centuries. Conversion to calendar ages before present (B.P., defined as 1950) was performed using CALIB5 (marine calibration curve 9.14c) (M. Stuiver, P. J. Reimer, and R. W. Reimer, CALIB radiocarbon calibration, execute version 5.0.2, http://radiocarbon.pa.qub.ac.uk/calib/, 2005). Errors, shown by 2σ ranges (Table 1), are related to the marked plateaus and nonunique solutions in the calibration procedure [*Stuiver and Reimer*, 1993].

[13] The alkenone unsaturation index, UK′37, was used to calculate sea surface temperatures (SST) following the calibration established by *Prahl et al.* [1988]. Details of the analytical procedure can be found in the work by *Sicre et al.* [1999]. Briefly, freeze-dried sediments were extracted with a mixture of 3:1 dichloromethane:methanol (v/v) in an ultrasonic bath for 15 min. The lipid extracts were then fractionated into compound classes by silica gel chromatography. The fractions containing alkenones were analyzed on a Varian Star 3400CX gas chromatograph equipped with a 50 m fused CP-Sil-5CB silica capillary column (0.32 mm i.d., 0.25 μm film thickness, Chrompack), a Septum Programmable Injector and flame ionization detector. The oven temperature was programmed from 100 to 300°C at 20°C min^{-1}. Helium was used as the carrier gas (25 mL min^{-1}). Quantification of individual alkenones was achieved by comparison of chromatographic peak areas with α-cholestane added prior to gas chromatography injection.

[14] 153 tephra grains were picked for elemental composition from four stratigraphic intervals showing elevated tephra concentrations (th1–th4). Individual grains were initially classified as black, grey, brownish translucent or colorless translucent. Elemental geochemistry was determined by wavelength dispersive microprobe analyses [*Mangerud et al.*, 1984]. Grains were selected to ensure that the range of visual types were represented, and prepared in polished epoxy discs coated with a 20 nm carbon layer. For each grain, at least three analyses were performed. The tephra material was generally of amorphous character. Heterogenic particle types with apparent porphyric texture were avoided due to poor analytical reproducibility. The raw data was converted to oxide percentages with mean and standard deviations calculated. Reproducibility was strongly dependent on elemental weight percentages, but typically better than ±2% for >10 wt.% and better than ±10% for 1–10 wt. %. Total oxides ranged from 97 to 99 wt. %. Low values are related to absorption of electrons during analyses or loss of Na due to evaporation.

4. Results

4.1. Geochronology

[15] Of the 12 AMS ^{14}C dates obtained from DA04-31P two shows stratigraphic inversions outside the range of analytical error (Table 1). Possible reasons for erroneous ages may relate to geological artifacts (i.e., reworking and bioturbation) or contamination during sample preparation. The sample at 156 cm depth (in the stratigraphic context some 8000 years "too old") was obtained from a more silty interval (Figure 3) possibly associated with enhanced sediment winnowing.

[16] An age model based on a nonlinear fit was constructed for the upper 3 m interval of core DA04-31P (Figure 2). Two functions were applied to fit the calibrated ^{14}C dating points (Figure 2a). An assumption of the age model is a decrease in sedimentation rates toward the core top (e.g., between the two dated horizons in the Holocene interval). Present-day low sedimentation rates are suggested by a marked Fe-oxide horizon developed in the upper 5 cm of the core (Figure 3). The ^{14}C based geochronology is supported by a pattern-based correlation between sediment bulk properties and the climate curve of the Greenland Summit ice cores (Figure 3 and Figure S1 in the auxiliary material).[1] Tephra horizons could not constrain the age model since volcanic material was associated with ice rafting (section 4.3). The 2 cm sampling interval gives a time resolution between 60 to 100 years in the glacial interval and between 100 to 1000 years in the Holocene section. Sedimentation rates are low in the uppermost late Holocene (<5 cm kyr^{-1}) and then subsequently increase with depth from 17 cm kyr^{-1} in the early Holocene to around 30 cm kyr^{-1} across the deglaciation.

4.2. Lithology and Bulk Sediment Properties

[17] A detailed lithostratigraphy of the core was achieved by continuous scanning for physical and geochemical properties. (Figure 3, entire core shown in Figure S1). The low background values of Ca (<7 cps) seen in most of the core corresponds to <5 wt. % $CaCO_3$ while the elevated cps counts in the upper 50 cm reflect carbonate values of 15–20 wt.%. Detrital carbonate horizons, related to Heinrich events HE 1 and HE 2, are very distinctive, forming sharp-based and top-down bioturbated, light beige layers matching Ca peaks (Figure 3). In contrast, HE 3 is vaguely defined by a thin beige interval and a Ca peak below a horizon dated to 26.2 ^{14}C kyr (Figure S1). The ^{14}C chronology of the detrital carbonate layers observed in DA04-31P is in agreement with the HE ages obtained from central North Atlantic cores [*Hemming*, 2004].

[18] The water depth of DA04-31P (~2500 m) is located at the interface between deep and intermediate boundary currents, which may explain the high glacial sedimentation rates compared to core sites located in the path of the DWBU [*Rahman and de Vernal*, 1994]. We observe a visual tie between measured sediment properties and the GISP2 $\delta^{18}O$ record that supports the ^{14}C based chronology (Figure 3 and Figure S1). Increases in GR density, and the minor elements Ba, Sr and Zr tend to correspond to warm intervals in GISP2. The changes in bulk parameters may reflect variations in fine-clastic mineralogy or water mass conditions, but the significance of geochemical variables in terms of climate variability requires more specific analytical information.

4.3. Ice-Rafted Detritus and Tephra

[19] IRD abundance is considered as an indicator of iceberg productivity reflecting gross ablation of marine-based

[1] Auxiliary materials are available in the HTML. doi:10.1029/2010PA002053.

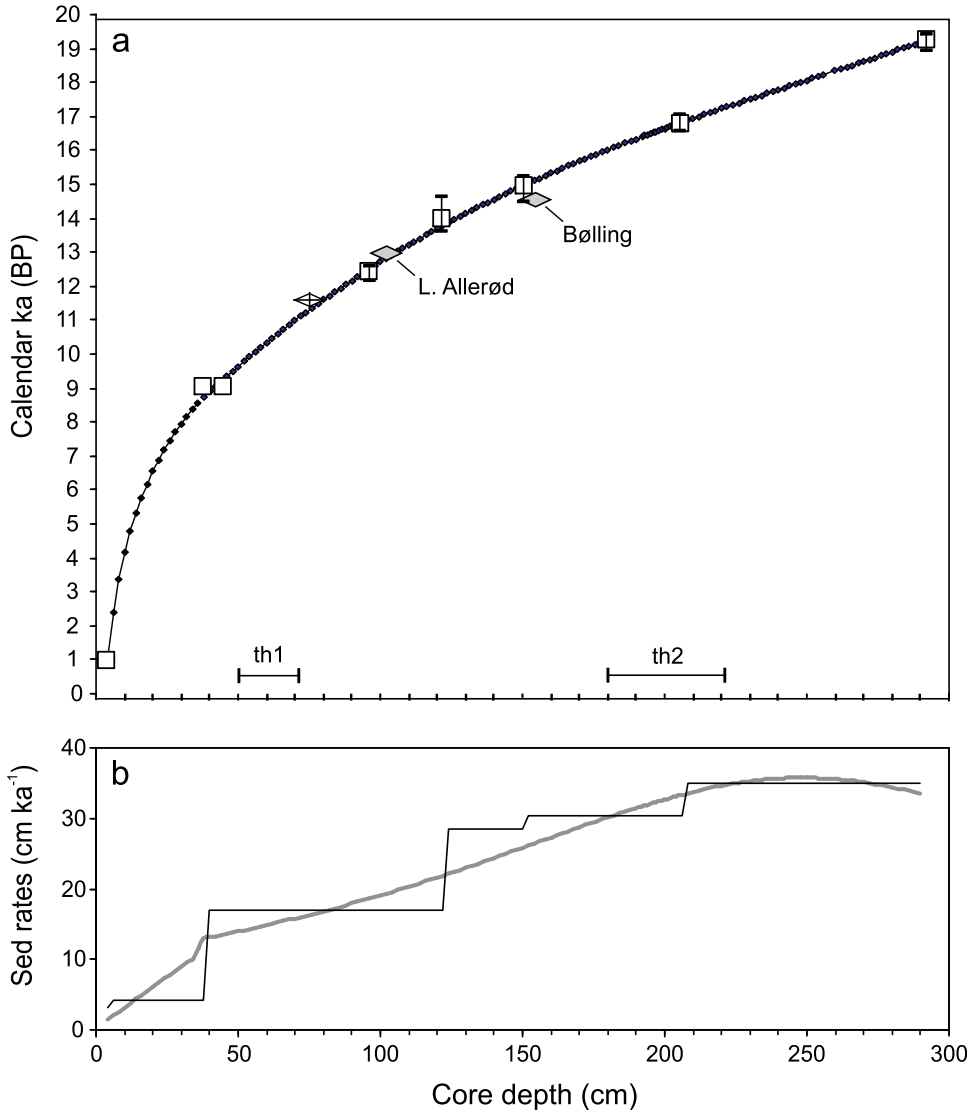

Figure 2. (a) Calendar age model for core DA04-31P based on a nonlinear function fit to calibrated AMS ^{14}C dates (open squares). The 2σ intervals of calibrated ages from Table 1 are indicated. Two algorithms were used: 3450Ln x - 3790 for the interval 4–36 cm and 0.00037 x^3 − 0.2768 x^2 + 96 x + 5460 for the interval 38–292 cm. Solid diamonds represent visual ties to the Bølling peak in the GISP2 ice core (Figure 3). Crosshair indicates position of the pre-Boreal increase in ocean temperature (Figure 4f). Also shown are the stratigraphic positions of tephra horizons th1 and th2. (b) Sedimentation rates based on linear interpolation between dating points (grey line) and using the nonlinear fit described above (black line).

ice sheets. Additional factors include variability in glacial debris concentration, iceberg melting rates and background sediment fluxes [e.g., *Alley et al.*, 2010]. Abundance of ice-rafted components determined in the deglacial section of DA04-31P is shown in Figure 4, together with other paleoenvironmental proxies. The results are compared to the Greenland oxygen isotope records (GISP2 and NGRIP, Figure 4f) on independent time scales. The total abundance of IRD > 250 μm reflects the flux of melting icebergs to the southwest Greenland margin (undifferentiated sources), while the abundance of detrital carbonate (DC) identifies icebergs derived from the LIS [*Andrews and Tedesco*, 1992] (Figure 4a). HE 1 is clearly seen as an interval of elevated DC abundances (10–35 grains g^{-1}) expressed by a jagged peak between 16.4 and 16.8 ka B.P. that is likely influenced by bioturbation observed in the top of the detrital carbonate horizon (Figure 3). From about 16 ka and throughout the remaining deglacial interval, DC grains are present in trace amounts only. The exact timing of HE 1 is difficult to place due to age model uncertainties (notably marine reservoir effect) but a duration of about 600 years implied by our results is in agreement with previous studies based on U-Th sedimentation rates [*Veiga-Pires and Hillaire-Marcel*, 1999].

[20] In addition to the HE 1/early deglacial interval, elevated IRD concentrations (50–150 grains g^{-1}) are observed

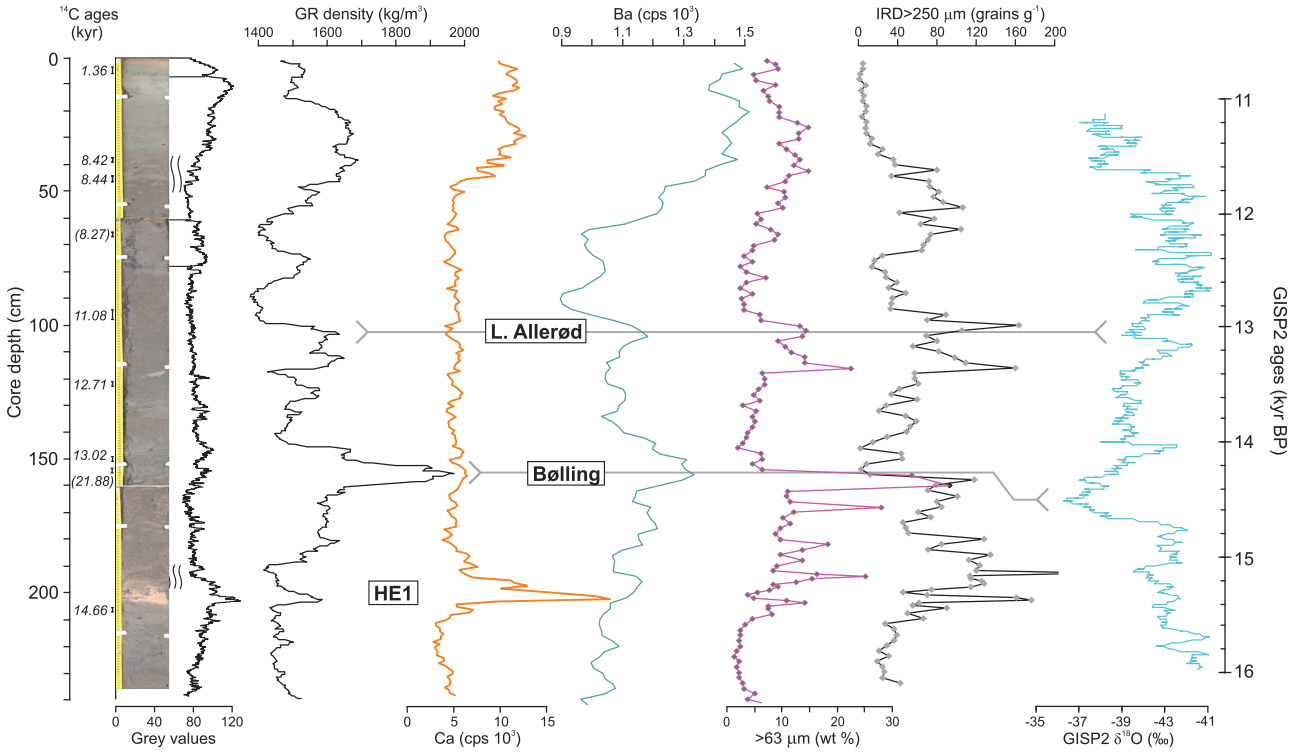

Figure 3. Lithology, XRF scanning, and other bulk sediment properties of the deglacial section of DA04-31P. Bioturbated intervals are noticed in the top of HE 1 and in the early Holocene interval (35–55 cm core depth). Positions of ^{14}C ages are indicated (age inversions in brackets). Peaks in bulk density and Ba are visually correlated to Bølling and late Allerød interstadial events in the GISP2 ice core.

in the pre-Bølling (15.2–15.8 kyr), Allerød to early Younger Dryas (12.4–13.6 kyr) and early Holocene (9.0–11.2 kyr) intervals (Figure 4a). Composite quartz aggregates and single-grain amphiboles are seen as significant subsidiary components in these intervals (Figure 4b) presumably related to glacial weathering of Achean and early Proterozoic gneisses in southern Greenland (Figure 1) [*Verplanck et al.*, 2009]. A similar locally derived, igneous petrology characterizes IRD composition during the early Holocene. In comparison, dredge samples from a seamount located northwest of DA04-31P show large amounts of rocks and pebbles dominated by Precambrian gneisses with no, or subordinate, presence of basalt and limestone [*Larsen and Dalhoff*, 2006]. We also note that olivine basalt material, despite being an abundant component in core and dredge samples from the Davis Strait (TTR-462G, Figure 1) is not identified in DA04-31P.

[21] Increased concentrations of glassy tephra are observed in two horizons of the deglacial interval: 50–70 cm (th1) and 180–224 cm (th2) corresponding to 16.0–17.2 kyr and 9.6–11.0 kyr (Figure 4c). High tephra abundances were also noticed at deeper intervals of the core, e.g., around 582 (th3) and 735 cm (th4). Images of the different tephra types that were identified visually are shown in Figure S2 in the auxiliary material. The majority of volcanic particles are translucent brown with broken bubble-wall, threaded or blocky morphologies, forming basaltic or intermediate compositions (section 4.7). Clear translucent and winged shards, related to rhyolitic lavas, are observed primarily in the younger th1, while grey pumice and black grains with conchoidal fractures are mainly observed in th2. The high tephra concentrations of th2 embrace the detrital carbonate horizon of HE 1, presumably caused by dilution from detrital IRD sources (Figures 4a and 4c). The increase in tephra grains from 17.2 kyr B.P. leads the onset of HE 1 with some 400 years. Even though late Quaternary eruptions may have been more powerful and wind patterns different from today, the distance of DA04-31P to the Icelandic sources makes in situ aeolian deposition unlikely for tephra >250 μm [*Lacasse*, 2001]. Rather, its association with siliciclastic detritus favor transport by floating icebergs, which also explains an "older-than-stratigraphic" age for some of the tephra components (section 4.7).

4.4. Biogenic Constituents

[22] In most of the analyzed section of DA04-31P foraminifer shells are a minor component of the sand fraction, although elevated concentrations are seen at the onset of HE 1 and during the early Holocene (Figure 4d). The foraminifer assemblage in DA04-31P is dominated by Neogloboquadrina pachyderma sinistral (Nps) considered as an indicator for polar water mass conditions (<5–7°C, salinity >34‰) [*Johannessen et al.*, 1994]. This deep-dwelling planktonic species occupy the water column from the chlorophyll maximum, 20–80 m below the surface, and down to the pycnocline, typically at 100–200 m water depth, where the shell density increases by addition of a calcite crust [*Kohfeld et al.*,

1996]. Despite its affinity to polar waters, conditions related to upwelling may also determine Nps abundances [*Ufkes et al.*, 2000]. Parts of the deglacial interval show a rich presence of diatom flora, mainly of the cosmopolitan species Coscinodiscus asteromphalis (Figure 4d). High concentrations of diatoms (classes 4–5) are observed across the transition into Bølling and during the pre-Boreal interval (10.5–9.5 kyr B.P.).

4.5. Stable Isotopes

[23] The $\delta^{18}O$ composition of Nps is determined by regional salinity and temperature changes of thermocline

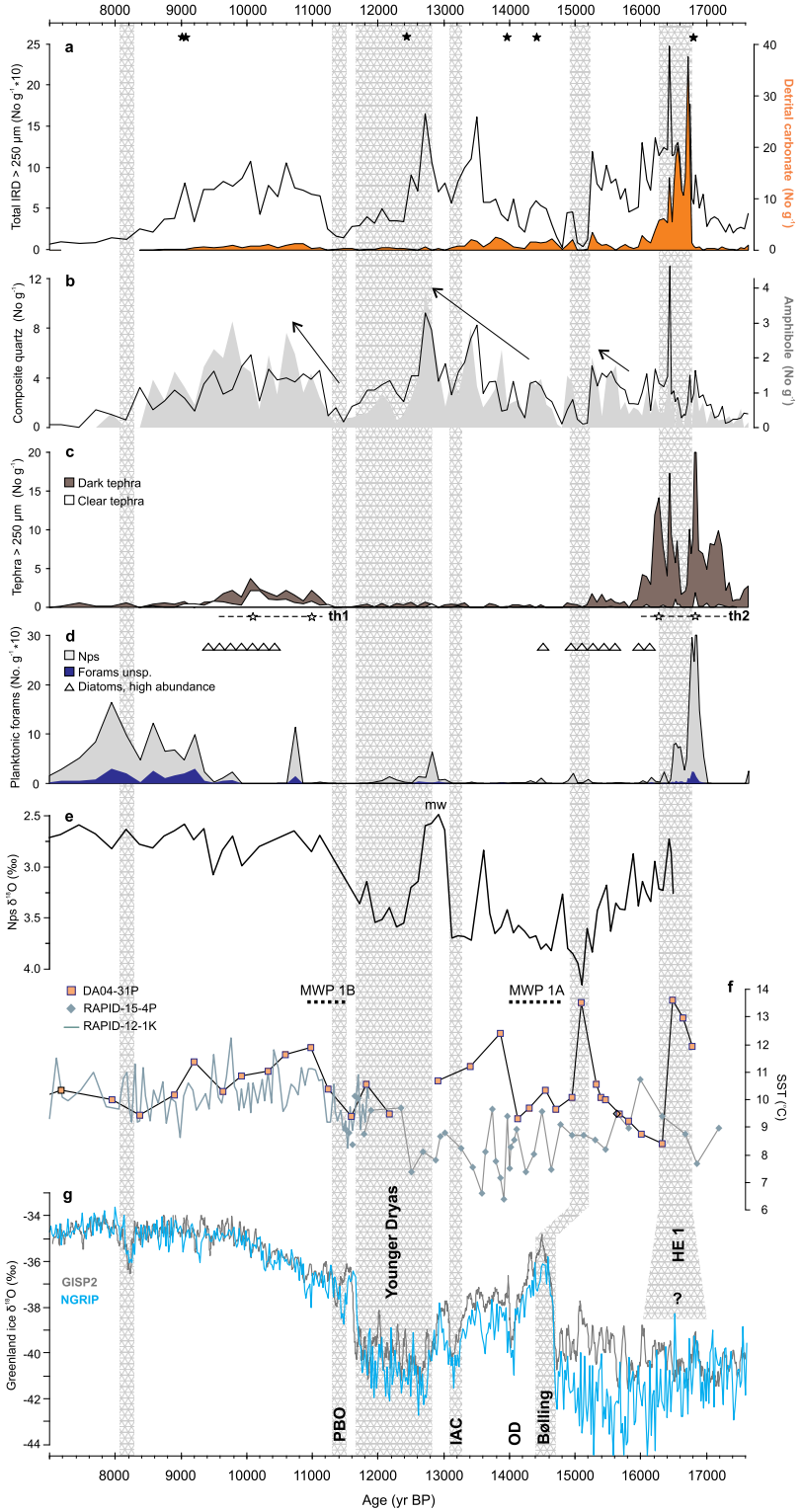

Figure 4

waters (~0–200 m), which are superimposed on the global seawater signal related to ice volume [*Shackleton*, 1987]. The δ^{18}O record from core DA04-31P show an increase from 3.2‰ at the termination of HE 1 to a maximum of ~4.0‰ at the onset of Bølling (Figure 4e). This transition corresponds to a stepwise reduction in IRD abundance and gradually increasing alkenone temperatures (Figure 4f). From the Bølling δ^{18}O maximum a general decrease is observed through the late deglaciation, leveling out in the early Holocene interval to an average of 2.75‰. This deglacial trend, also seen in previous studies, is attributed to a combination of increasing sea surface temperatures and the transfer of isotopically light meltwater from decaying ice sheets into the oceans [*Rahman and de Vernal*, 1994; *de Vernal and Hillaire-Marcel*, 2000]. In addition, we observe three discrete δ^{18}O depletions through the Bølling-Allerød interval. This is most noticeable by a 1.2‰ shift at 13 kyr with values returning to base level during the first half of Younger Dryas. The two most significant δ^{18}O depletions correlate with elevated IRD concentrations (and are therefore related to melting icebergs) and the warm intervals of the Allerød period in the Greenland ice cores (Figure 4g).

4.6. Alkenone SST Data

[24] C_{37} alkenone concentrations were generally low, ranging in mean values from 3.5 ng g^{-1} during deglacial, to 12 ng g^{-1} during the Holocene. Such low abundances are not unexpected from polar ocean regions and have been reported earlier in seafloor sediments and surface waters [*Sikes et al.*, 1997; *Sicre et al.*, 2002]. In the Southern Ocean, the observation of increasing abundances with decreasing latitude (hence increasing water temperature) led to the conclusion that production likely reflected factors such as better light conditions and a longer growth season [*Sikes et al.*, 1997]. Immeasurable alkenone levels were found at sites with summer temperatures cooler than 4°C and usually covered with winter sea ice. Similar environmental parameters likely explain the low concentration levels in the deglacial interval of core DA04-31P.

[25] Alkenone temperatures recorded in DA04-31P range between 8° and 14°C with four peaks/intervals >11°C (Figure 4f), which compared to present SST's of 3–8°C in the northern Labrador Sea seems excessive. In low productivity regions such as the Labrador Sea, lateral advection of detrital alkenones can represent a significant component of surface sediments. Earlier studies suggest that alkenones drifting with strong surface currents can potentially generate significant deviation from in situ SSTs [*Sicre et al.*, 2005; *Rühlemann and Butzin*, 2006]. Higher than expected values in DA04-31P may therefore point to a contribution of alkenones that were produced in distant warmer waters. Since the alkenone-based temperatures are derived from bulk samples it is likely that the obtained signal reflect algeal compounds carried westward into the Labrador Sea by the Irminger Current. Presently, cocolithophorid blooms south of Iceland represent a potential primary source of algeal material entrained by the Irminger Current. Previous studies in the North Atlantic have observed sedimentary SST anomalies several degrees higher than measured in seawater at the end of the growing season [*Conte and Eglinton*, 1993; *Bendle and Rosell-Mele*, 2004]. Acknowledging this factor we interpret the alkenone data as a tracer of water masses derived from Irminger Current transport rather than indicating true local SST.

[26] The transportation history of algeal material from their source regions (e.g., pelagic, along-slope currents, nepheloid layer) is speculative but in any case, the enhanced sedimentation rates of DA04-31P facilitate fast burial of algae compounds. To gain further insight we compare the alkenone record with Mg/Ca-based SST data from core sites in vicinity of the main branch of the North Atlantic Current (RAPID site shown in Figure 1) [*Thornalley et al.*, 2009, 2010]. The remarkable agreement between the two SST proxies throughout the Holocene interval (Figure 4f; see Figure S3 for entire record) favor a coherent upper ocean circulation driven by Irminger Current activity since the pre-Boreal. In contrast, digressions between the two SST records through the deglacial period suggest that Atlantic surface circulation was markedly different from the present.

4.7. Tephra Geochemistry

[27] Our analyses include tephra material extracted from the pre-LGM interval of DA04-31P (Figure 5; geochemical data included in Table S1) although here we focus on the elemental compositions of basaltic tephra from th1 and th2, forming part of the deglaciation history (Figure 6; see Table S2 for comprehensive tephra references). The elemental compositions are discussed in the context of volcanic source but bearing in mind that the tephra particles are related to ice transport rather than direct atmospheric fallout.

[28] The compositions of tephra are consistent with Icelandic volcanic sources characterized by transitional alkali-basaltic and tholeiitic compositions [*Kvamme et al.*, 1989; *Wallrabe-Adams and Lackschewitz*, 2003] (Figure 5). Only few data points are observed that potentially could relate to other volcanic regions like Jan Mayen (trachybasalt),

Figure 4. Proxy data from upper section (0–230 cm) of core DA04-31P and correlation with Greenland ice core data on a calendar time scale (positions of ^{14}C dates indicated by stars). (a) Total IRD and detrital carbonate abundances (orange fill). (b) Abundance of composite quartz, representing quartz-plagioclase-amphibole aggregates (black line), and black amphibole grains (grey shaded curve). Arrows denote stages of increasing trends in IRD. (c) Abundance of light, rhyolithic, and dark basaltic tephra. Open stars denote tephra sampling horizons. (d) Abundance of *N. pachyderma* sinistral (Nps) and unspecified planktonic foraminifera. Intervals with high relative abundances of diatoms (classes 4–5) are indicated by triangles. (e) Stable isotope data δ^{18}O measured on Nps and calibrated to the VPDB standard. (f) Marine temperature data (SST) derived from alkenone saturation index (this study) and Mg/Ca measurements (*G. bulloides*, 0–50 m water depth) extracted from RAPID cores (Figure 1) [*Thornalley et al.*, 2009, 2010]. Position of MW1A and 1B are indicated [*Bard et al.*, 1996; *Stanford et al.*, 2006]. (g) The δ^{18}O from the central Greenland ice cores GISP2 and NGRIP [*Meese et al.*, 1997; *Rasmussen et al.*, 2006].

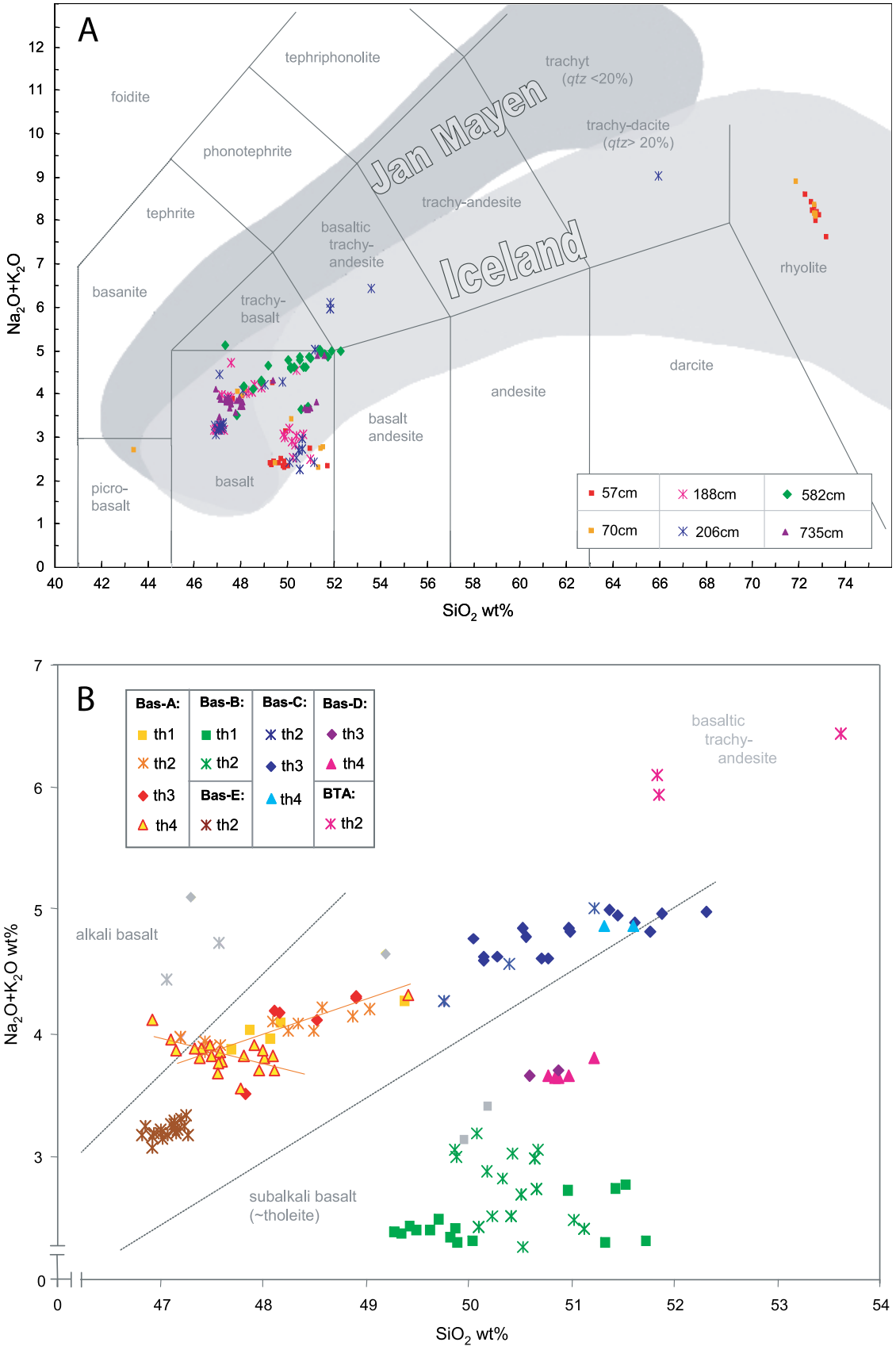
A
tephriphonolite
trachyt
(qtz <20%)
foidite
Jan Mayen
trachy-dacite
(qtz> 20%)
phonotephrite
trachy-andesite
tephrite
basaltic
trachy-
andesite
Iceland
rhyolite
basanite
trachy-
basalt
darcite
andesite
basalt
andesite
basalt
picro-
basalt
57cm
188cm
582cm
70cm
206cm
735cm
Na2O+K2O
SiO2 wt%
B
Bas-A:
th1
th2
th3
th4
Bas-B:
th1
th2
Bas-C:
th2
th3
th4
Bas-D:
th3
th4
Bas-E:
th2
BTA:
th2
basaltic
trachy-
andesite
alkali basalt
subalkali basalt
(~tholeite)
Na2O+K2O wt%
SiO2 wt%

Figure 5

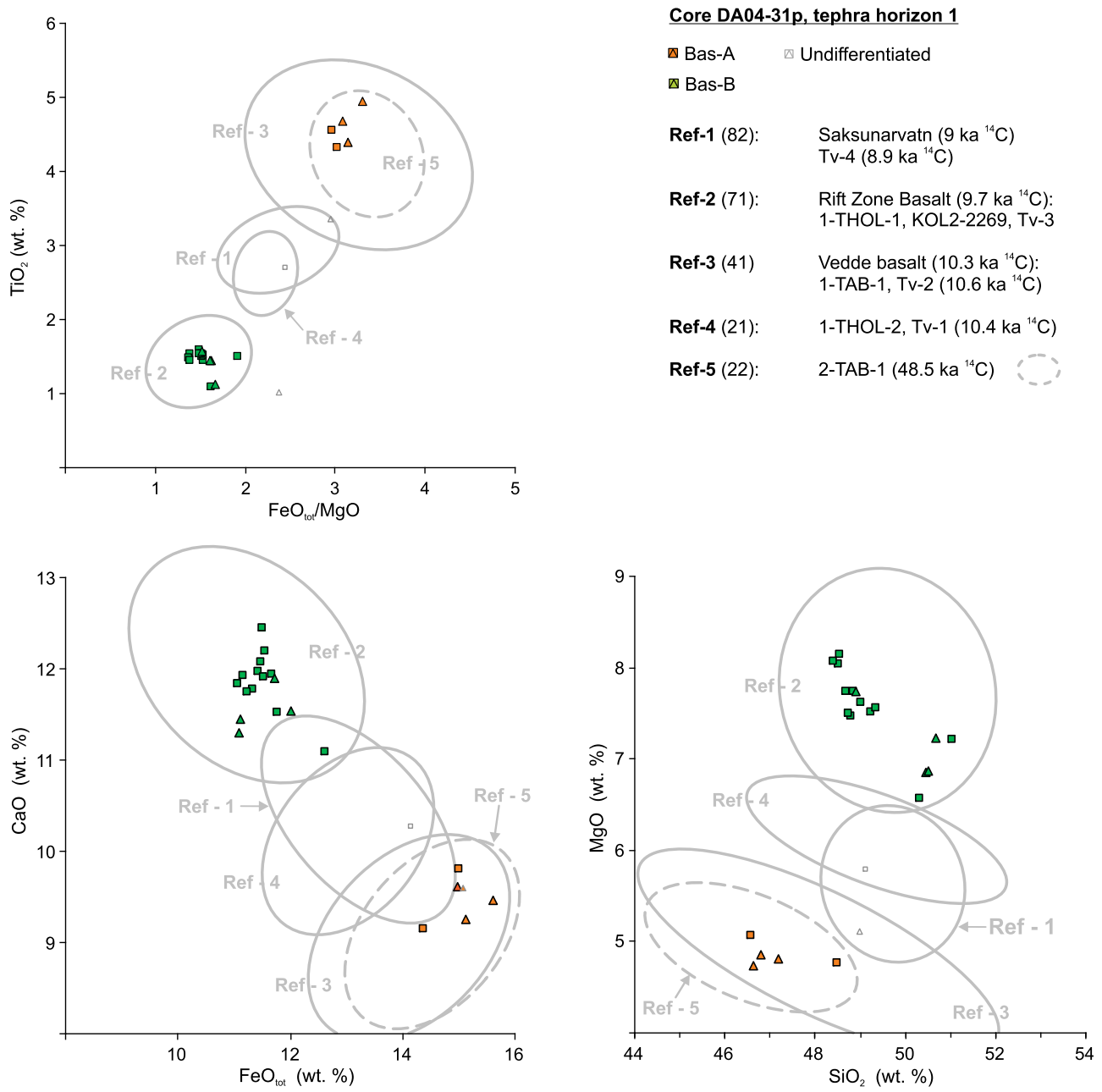

Figure 6. Selection of elemental crossplots for tephra horizons 1 and 2 (positions shown in Figure 4). Basaltic subgroups (A-E, BTA) are compared to known North Atlantic ash layer compositions (grey circles). Each circle encloses data points for particular volcanic events based on a large number of references (see Table S2 for details of reference groups). "Undifferentiated" represents data points that do not conform to any of the six basaltic types. Ref-5 (hatched circle) corresponds to NAAZ-2.

Figure 5. Total alkali versus silica (TAS) composition of tephra particles analyzed from core DA04-31P. (a) Full range of tephra compositions with signature of data points referring to sample depths in the core (Figure 3 and Figure S1). General geochemical trends are indicated representing magmatic evolution in Iceland and Jan Mayen. (b) Detail of basaltic TAS range with data points referring to basalt type (Basalt A-E and Trachy-Andesite) as well as tephra horizons in the core. The distribution show a clear distinction between tephra of intermediate basaltic composition and subalkali basalt derived from tholeiitic magmas, characterizing the Icelandic Rift zone eruptions [*Lackschewitz and Wallrabe-Adams*, 1997]. For the Bas-A cluster, a delineation of trends is indicated by the thin red lines. Grey markers represent single data points that cannot be matched with any of the six subgroups ("undifferentiated" in Figure 6). The tight cluster of low-alkaline/low-silica data points forming the Bas-E type is only observed in th2.

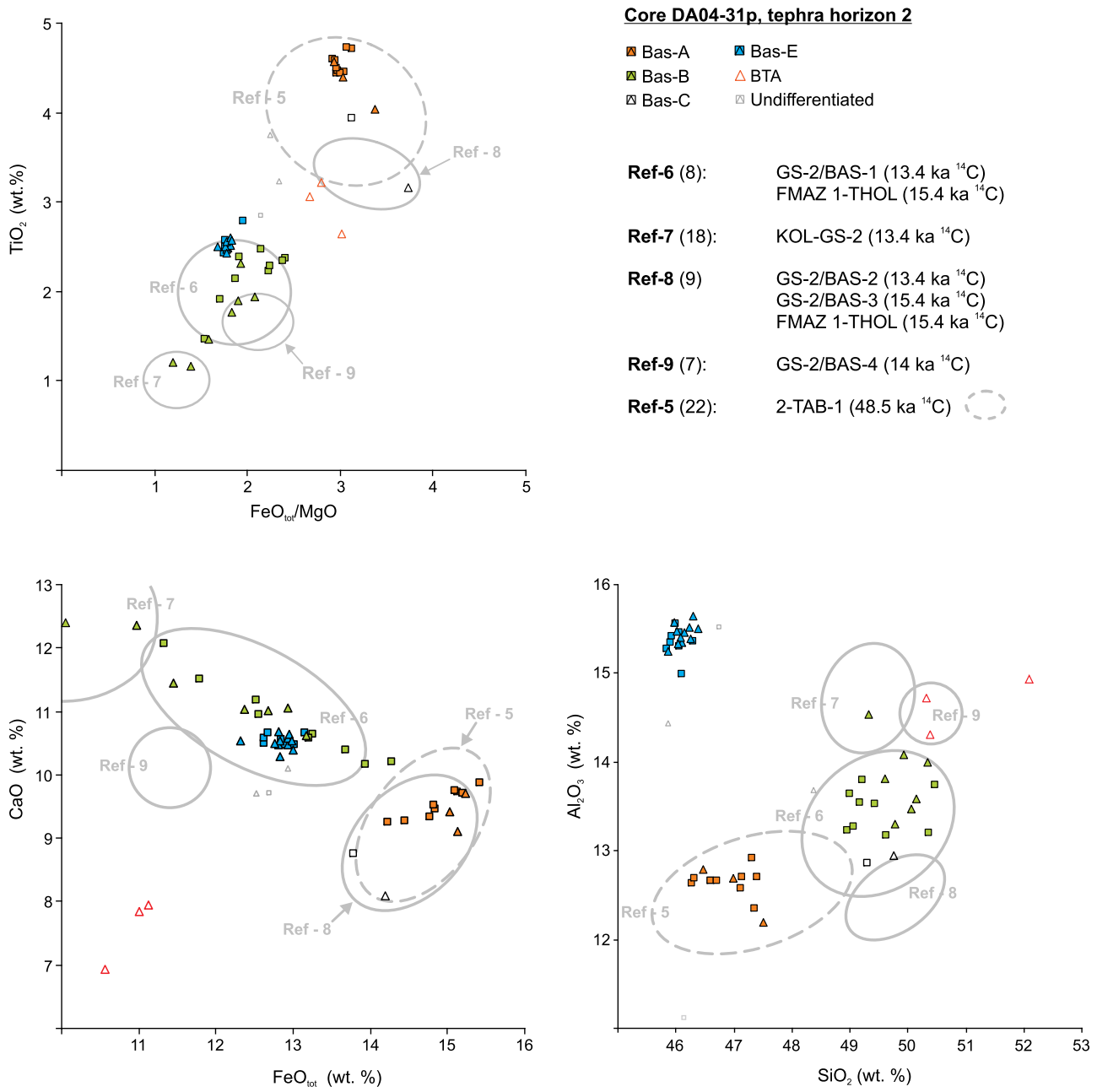

Figure 6. (continued)

Azores (trachytic) and Laacher See (phonolitic). Th1 contains Si-rich tephra appearing as translucent "winged" shards under the microscope. This population corresponds geochemically to the Vedde rhyolitic component of the North Atlantic Ash Zone 1 (NAAZ-1) widely described in the North Atlantic region [*Ruddiman and Glover*, 1972] and referred to as I-RHYL-1 by *Kvamme et al.* [1989]. Out of the 42 grains measured from th1, 12 were of a rhyolitic composition. In comparison the ratio between light and dark tephra in the grain counts is 1:2.

[29] The basaltic tephra from th1 clusters in two groups, denoted Bas-A and Bas-B with a dominance of the latter (~70%) (Figure 5b). Bas-B, of tholeiitic composition, corresponds to the I-THOL-1 population (Figure 6, th1) identified as a product of Icelandic Rift Zone volcanism dated in lake sediments to between 10 and 11 kyr [*Björck et al.*, 1992]. The Fe-rich Bas-A component correlates with the Vedde basaltic ash I-TAB-1 dated in marine cores to 11–12 kyr [*Kvamme et al.*, 1989; *Kristjansdottir et al.*, 2007]. In comparison, the GRIP ice core contains a minor population of Vedde ash grains dated to 11,980 yr B.P. [*Gronvold et al.*, 1995]. High Ti/Ca also applies to basaltic tephra of the much older NAAZ-2 (52–53 kyr B.P.) [*Kvamme et al.*, 1989], but the coincidence of Bas-B with a rhyolitic component points to the Vedde eruption at the end of the Younger Dryas (Figure 6, th1). Both basaltic populations in th1 cor-

respond to NAAZ-1 commonly observed in North Atlantic cores [*Ruddiman and Glover*, 1972; *Kvamme et al.*, 1989]. A signature of 1-THOL-2 and the early Holocene Saksunarvatn eruption that produced a prominent ash layer in Iceland several centuries after the 1-THOL-1 event [*Björck et al.*, 1992] has not been identified. Bas-B, at the onset of th1 (Figures 4 and 6), coincides roughly with the timing of Icelandic Rift eruptions associated with 1-THOL-1 (9.7 ^{14}C kyr) [*Björck et al.*, 1992]. However, Bas-B shows a delay of about 1000–1500 years compared to its assumed terrestrial equivalent (Vedde basalt at 10.3–10.6 ^{14}C kyr). This inconsistency and the extended interval of tephra deposition across the pre-Boreal are inferred to reflect a combination of ice storage/transport and vertical mixing by bioturbation [*Ruddiman and Glover*, 1972].

[30] Analytical results from th2 show three main basaltic populations, Bas-A (25%), Bas-B (30%) and Bas-E (33%) and minor contributions from other populations (Figure 5b). The best match for Bas-B at the stratigraphic interval of th2 (16–17 kyr) is the ash zone FMAZ I-THOL reported by *Wastegård et al.* [2006] (Figure 6, th2). This ash zone is identified in marine cores from the northeast Faeroese shelf and is dated to 15.4 ^{14}C kyr. The Bas-E population is marked by a high Al content (Figure 6, th2) and very homogeneous composition of low Si and transalkali elements (Figure 5b). This composition it is not clearly recognized in previously published studies of MIS-2 tephra horizons. A tephra population from Reykjanes Ridge cores [*Lackschewitz and Wallrabe-Adams*, 1997] shows a cluster similar to Bas-E based on the TAS composition although the Al content was not reported. For Bas-A, the only compositional match with previous published tephra data older than HE 1 is the trans-alkali basalt population of NAAZ II [*Wastegård et al.*, 2006], suggesting a 35 kyr delay from time of eruption (Figure 6, th2). We infer that this tephra material was stored as englacial debris in marginal ice sheets and released during the early deglaciation and HE 1 together with igneous basal debris.

5. Discussion

5.1. Glacial Sources for Ice-Rafted Debris

[31] Heinrich events (HE) are commonly observed in North Atlantic cores as centimeter-thick layers containing ice-rafted detrital carbonate clasts observed as far as the West European margins [*Zahn et al.*, 1997; *Knutz et al.*, 2007]. The detrital composition is related to glacial erosion of Paleozoic limestone in the Hudson Bay and its peripheral regions, e.g., Foxe and Emerald basins [*Hemming*, 2004]. On the east Canadian slope in vicinity of the NAMOC channel, HE 1 and HE 2 are represented by 1–3 m thick intervals of beige-colored graded muds interpreted as turbidites and meltwater plumites [*Rashid et al.*, 2003]. The character of these deposits, in a proximal location to the glacial source, combined with the strong ocean-wide δ^{18}O depletions in planktonic shells, testify to the massive outbursts of meltwater from the LIS [*Bond et al.*, 1993]. Thus, the detrital carbonate horizons in DA04-31P are a signature of these immense ice-laden meltwater plumes that inundated the continental margin of southwest Greenland (Figure 3 and Figure S1). Conversely, the lack of a detrital carbonate peak, corresponding to HE 0 [*Andrews et al.*, 1995], imply a limited influence of LIS icebergs on the West Greenland margin during Younger Dryas [see also *Andrews and Tedesco*, 1992]. Likewise, a carbonate horizon associated with HE 3 is only faintly visible in the core lithology. This suggests that only during major LIS collapses did icebergs produced from the Hudson Channel reach the Greenland margins, located "upstream" with respect to the prevailing boundary currents. We infer that the most probable source of the immature siliciclastic IRD material in DA04-31P relates to erosion of Archean-early Proterozoic gneisses in southern Greenland [*Verplanck et al.*, 2009]. The study site would monitor nearby calving fronts in southwest Greenland margin as well as icebergs drifting with the East Greenland Current into the northern Labrador Sea (Figure 1).

5.2. Evidence of Deglaciation in Southern Greenland

[32] Despite considerable uncertainty pertaining to the timing and extent of the LGM Greenland Ice Sheet, most data and models support a shelf edge configuration [*Funder et al.*, 2004; *Ó Cofaigh et al.*, 2004; *Roberts et al.*, 2008]. The maximum volume, estimated to 4.6 m of excess ice-equivalent sea level, may not have been reached before 16.5 kyr [*Simpson et al.*, 2009]. In southwest Greenland, the LGM stage has been associated with the Hellefisk Moraine forming the present topographic highs of the middle to outer shelf [*Funder et al.*, 2004]. Estimates of LGM ice thickness range from 700 to 1000 m in the outer fjord regions of Sisimiut [*Rinterknecht et al.*, 2009] to >1500 m along the southern coastal fringe [*Bennike et al.*, 2002].

[33] Dating of marine cores from the southeast Greenland shelf and slope suggests a minimum age of 14.5–16.0 kyr B.P. for the onset of ice retreat [*Kuijpers et al.*, 2003; *Jennings et al.*, 2006]. This early deglacial phase is associated with elevated concentrations of ice-rafted material in the pre-Bølling interval of core DA04-31P, 16.0–17.4 kyr (Figures 4a–4c). The pronounced increase in ice-rafted basaltic tephra around HE 1, which includes a significant NAAZ-II component (about 25% of data points in th2) (Figure 6, th2), indicates iceberg transport from southeast Greenland and the Denmark Strait region, in proximity to the Icelandic source. It is considered unlikely that NAAZ-II ash was locked in semipermanent sea ice for 35 kyr, and nor does the dynamic Icelandic Ice Sheet appear as a suitable candidate for long-term ash storage. The other possibility is that Icelandic tephra was stored in glaciers covering the east Greenland margin shelf terminating in floating ice shelves. The coeval supply of siliciclastic IRD in DA04-31P and the findings of dislocated ash in cores from the Kangerlussuaq Trough (Figure 1) [*Jennings et al.*, 2002] support an origin from east Greenland. Transport of tephra-rich icebergs by the Greenland coastal current is corroborated by results from core SU90-24 (Irminger Basin, Figure 1) showing a distinct double peak with high concentrations of dark volcanic ash and a marked δ^{18}O meltwater pulse at ~17 kyr (i.e., at the onset of HE 1) [*Elliot et al.*, 1998]. The decrease in δ^{18}O seen in the pre-Bølling interval of DA04-31P (Figure 4e) likely corresponds to the terminating limb of this meltwater peak. We infer from these observations that breakup of buttressing ice shelves on the east Greenland margin began prior to 17 kyr and lasted for several hundreds of years. It appears that the production of GIS icebergs was intermittently reduced during HE 1 but the subsequent increase in tephra abundances points to a prolonged early deglaciation

phase. By Bølling time the eastern fringe of the GIS had experienced significant decay, which may explain the lack of ice-rafted tephra in DA04-31P corresponding to the ash horizon between 14.0–14.8 kyr seen in the NGRIP ice core [*Mortensen et al.*, 2005].

[34] Several studies suggests that a major part of deglacial retreat in south Greenland occurred between 12 and 14 kyr, presumably in response to interstadial warming [*Bennike and Björck*, 2002]. The trend of ice margin recession was not continuous but interrupted by one or more readvances, documented by the Sisimiut Moraine on the innermost shelf [*Bennike et al.*, 2002; *Rinterknecht et al.*, 2009], Milne Land moraines in Scoresby Sund [*Miller*, 2008] and development of weathering boundaries in south Greenland (Neria stade) [*Weidick et al.*, 2004]. Due to the problems of dating till records and submerged morainal ridges, the timing of renewed ice sheet expansion is not well constrained but linkages to the pre-Boreal Oscillation and the Younger Dryas cooling have been suggested [*Alley et al.*, 2010]. The record from DA04-31P display an increasing trend in IRD abundance from the Bølling warm peak to the onset of Younger Dryas, suggesting enhanced supply of melting icebergs to the northeast corner of the Labrador Sea. In contrast, low IRD concentrations mark the later part of Younger Dryas, which may suggest a cold ocean climate with dense sea ice (sikussak) constraining the seaward mobility of icebergs [*Reeh et al.*, 1999]. Although our marine data cannot directly monitor increasing ice volumes, we suggest that the reduction in IRD abundance after 12.4 kyr B.P. is associated with an increase in gross mass balance and formation of new stillstand limits on the continental shelf. A similar interpretation may pertain to the low IRD concentrations during Oldest Dryas and the intra-Allerød Cooling (Figure 4).

[35] Seafloor observations from east Greenland margins indicate a stage of rapid ice stream retreat [*Syvitski et al.*, 2001; *Dowdeswell et al.*, 2010] lasting until 13–12.5 kyr [*Kuijpers et al.*, 2003; *Ó Cofaigh et al.*, 2004]. This event is possibly associated with the pronounced IRD peaks and δ^{18}O depletion spikes seen in DA04-31P between 13.6 and 12.6 kyr. A major recessional phase during Allerød is commensurate with dated sedimentary records from the Kangerlussuaq Trough (Figure 1) [*Andrews et al.*, 1997; *Jennings et al.*, 2006], although in the study by Jennings et al. the meltwater signal occurs 200–300 years later than in DA04-31P. However, considering the uncertainties pertaining to ^{14}C age calibrations it is equally possible that the two localities record a synchronous deglacial response.

[36] During the early Holocene optimum the GIS shrank beyond its present-day limits, possibly by up to 60 km inland in southern regions [*Tarasov and Peltier*, 2002]. In DA04-31P this final deglacial stage correlates with a broad IRD increase starting at the pre-Boreal Oscillation (Figure 4). The gradual decrease in IRD from about 10 kyr B.P. is consistent with near-field observations suggesting that glaciers in southern Greenland emancipated outer fjord systems between 8 to 11 kyr B.P. [*Bennike and Björck*, 2002; *Rinterknecht et al.*, 2009].

5.3. Oceanic Factors for Greenland Ice Sheet Instability

[37] Ice sheet surging has been proposed as a mechanism for Heinrich events, but the seaward delivery of large amounts of debris in a wet-based fast flowing glacier is problematic and in general not supported by observations [e.g., *Kamb*, 2001]. Moreover, glaciological models contest a full-scale surging behavior of the GIS [*Tarasov and Peltier*, 2002]. An alternative hypothesis links the North Atlantic evidence of periodic IRD fluxes to disintegrating ice shelves [*Hulbe*, 1997] that extended the Quaternary ice sheets into deep-water regions, similar to present-day ice shelves around Antarctica. We consider that collapses of marine-based glacial margins, promoted by climate-related factors, presents the most feasible explanation for elevated IRD concentrations in DA04-31P.

[38] A potential trigger for glacial margin collapse is related to global sea level rises, causing detachment of glacial anchor points and a landward progression of the grounding line. Over the last deglaciation two events of rapidly rising sea levels have been identified, known as meltwater (MW) pulses 1A and 1B [*Fairbanks*, 1989; *Bard et al.*, 1996]. MW 1A has been associated with a 20 m increase in sea level over less than 500 years. Dating of corals and shelf sediments place the start of this event to between 14.0 and 14.6 kyr [*Hanebuth et al.*, 2000; *Stanford et al.*, 2006], i.e., the Bølling–Older Dryas transition, which in DA04-31P is marked by relatively low SSTs and a δ^{18}O depletion peak of ~0.5‰ (Figure 4). MW 1A occurs >500 years before the IRD event at 13.6 kyr, and therefore it seems unlikely that the GIS retreat leading up to Younger Dryas was induced by rapid melting of other ice sheets. The onset of MW 1B is not well-constrained from global records, but here a different case can be made since it overlaps the pre-Boreal IRD increase, thus identifying rising sea levels as a possible factor for the final glacial recession in south Greenland. However, the concomitant increase in both atmospheric and oceanic temperature (Figures 4f and 4g) complicates the cause-effect relationship for this part of the record.

[39] We interpret the alkenone SST record from DA04-31P as an indicator of subsurface ISW transport by the Irminger Current, which today has a major influence on ocean-climate conditions in southwest Greenland [*Holland et al.*, 2008]. ISW form a remnant of Subpolar Mode Water, i.e., warm water derived from the Gulf Stream, which has traveled cyclonically around the subpolar gyre at depths above 800 m [*McCartney and Talley*, 1982]. The potential temperature of Subpolar Mode Water, ranging from 8 to 12°C in its source regions [*McCartney and Talley*, 1982, Figure 6b], is consistent with proxy-based SSTs of 10–11°C in the late Holocene interval (Figure 4f).

[40] The alkenone SST record from DA04-31P imply a marked variability of ISW transport through the last deglaciation, with 8 data points >10.5°C similar to, or exceeding, the early Holocene temperature anomaly (Figure 4f). This could mean that subsurface warm water transport to the Greenland margin during Bølling and Allerød was analogous to the early Holocene optimum. Despite the caveat of limited data (e.g., Bølling only defined by one data point), our results are consistent with the findings of enhanced Atlantic inflow along the northwest European margin during Bølling-Allerød [*Haflidason et al.*, 1995; *Rasmussen and Thomsen*, 2008]. Conversely, the RAPID study south of Iceland (Figure 1) show significantly reduced SSTs during the Bølling-Allerød interval [*Thornalley et al.*, 2010] and as such it differs noticeably from the North Atlantic climate

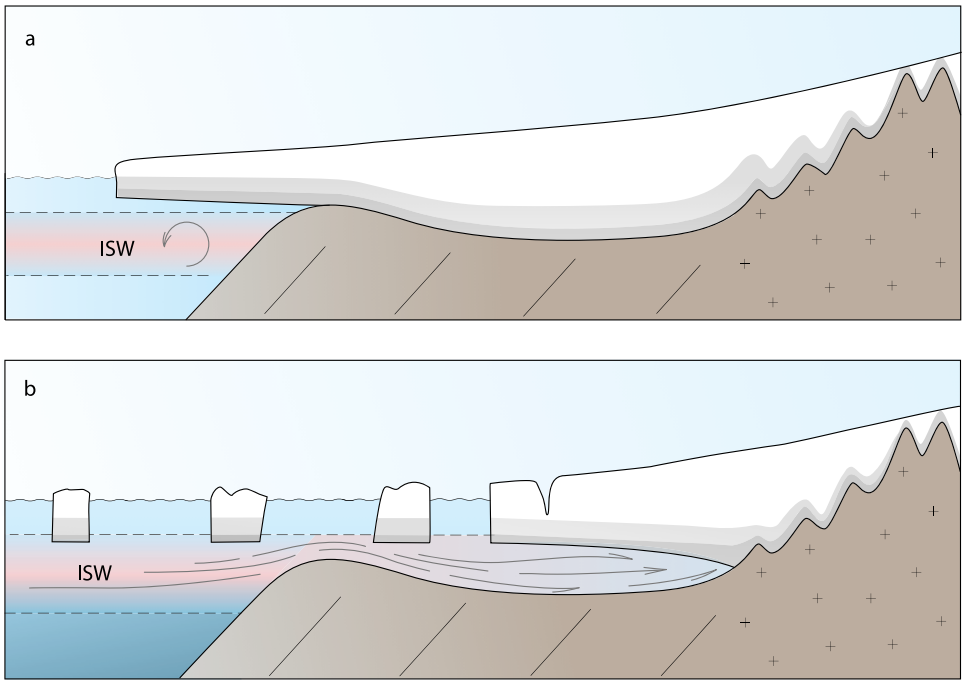

Figure 7. Model illustration of the relationship between subsurface warm water transport (ISW, Irminger Sea Water) and Greenland ice shelf disintegration. (a) In the maximum stage scenario, the base of the ice sheet at its marine limit (e.g., grounding line) is not in contact with ISW. (b) Fast deglacial retreat, associated with intense iceberg productivity, occurs when ISW invades the continental margin via the glacial troughs. Icebergs escaping the shallow grounds on the outer shelf are susceptible to transport by the prevailing boundary currents, thus allowing their cargo of IRD to be deposited at locations far from the source. Glacial mass loss is subsequently sustained by acceleration of ice streams as offshore anchor points buttressing the inland ice dome are being eliminated and the basal melting zone invades the deep fjord systems.

trend (Figures 4f and 4g). Based on salinity reconstructions *Thornalley et al.* [2010] associate the anomalous pattern with LIS freshwater emissions, conceivably entrained into the subtropical gyre and then advected northward by the North Atlantic Drift. Thus, it appears that deglacial upper ocean circulation in the northwest Atlantic was radically different to that of the Holocene. It is possible that Atlantic meridional inflow to the Labrador Sea followed a more southwesterly path due to a weak and diminished subpolar gyre. Moreover, during periods of high freshwater forcing the meridional transport from tropical source regions to high-latitude margins may have continued in the form of subsurface-intermediate water masses, i.e., at depths not necessarily recorded by planktonic foraminifer [e.g., *Rasmussen et al.*, 2003]. This glacial circulation mode is recognized by model simulations demonstrating that pooling of freshwater at midlatitudes can boost subhalocline heat transport during periods when intermediate ventilation is suppressed [*Knutti et al.*, 2004; *Mignot et al.*, 2007]. A hosing experiment by *Mignot et al.* [2007] applying freshwater at 50–80° N produced a maximum temperature anomaly (locally >8°C) penetrating into high latitudes at depths between 300 and 700 m. Despite uncertainties and need for further research, these results bolster our supposition that high alkenone values in DA04-31P are related to subsurface water mass transports.

[41] Observations from high-latitude fjord settings [*Holland et al.*, 2008; *Rignot et al.*, 2010; *Johnson et al.*, 2011] and the recent loss of West Antarctic ice shelves [*Shepherd et al.*, 2004] testify to the importance of ocean warming as a mechanism for glacial destabilization. *Knutz et al.* [2007] point to ocean heat transport and ice shelf instability as a trigger for northwest European iceberg discharges during MIS 2. *Alvarez-Solas et al.* [2010] invoke a similar mechanism for Heinrich events using ocean-climate modeling to demonstrate a causal linkage between subsurface ocean temperature increases and retreating ice shelves. In accord with *Jennings et al.* [2006] we propose that the deglacial retreat of the GIS was prompted by the incursion of warm subsurface ISW on the shelf margin (Figure 7). The observations from DA04-31P suggest that an increase in ISW transport started at the beginning of Allerød (~14 kyr), leading the first $\delta^{18}O$ depletion peak with 200–300 years and then followed by the main meltwater-IRD pulse 800–1000 years later (Figure 4). Thus, the effect of ISW on glacial mass loss was apparently not instantaneous but delayed with several centuries. This may reflect the time required for intermediate waters to enter the deep cross-shelf troughs beneath the floating ice shelf, after which, ice margin breakup can occur swiftly. We stress, however, that the centennial-scale response of the GIS to warm water advection is obscured by the lack of detail in the alkenone record.

[42] The early deglacial SST peak (11.9–13.6°C) at the base of HE 1 seems curious since it has no clear counterpart in the ice core signal (Figures 4f and 4g). Its correlation with

markedly increased Nps abundances may suggest favorable nutrient conditions linked with transient upwelling [*Ufkes et al.*, 2000]. This apparent subsurface pulse is commensurate with an ocean warming mechanism for Heinrich events [*Alvarez-Solas et al.*, 2010] although it requires approval from other sites.

5.4. The Younger Dryas Enigma

[43] The Younger Dryas cold reversal is arguably the most globally significant event of the last deglaciation [*Denton et al.*, 2005]. This return to stadial conditions, recorded in numerous terrestrial and marine archives, is notably linked to episodes of freshwater flooding affecting the poleward heat transfer by AMOC [*Broecker et al.*, 1988]. Modeling studies show that the suppression of meridional heat transport occurs most effectively when freshwater is released directly into areas of deep water convections, i.e., the Labrador Sea and the Nordic Seas [*Fanning and Weaver*, 1997], thus emphasizing meltwater sources in the western and northern North Atlantic.

[44] The most prominent source is related to catastrophic floods from the ice-dammed Lake Agassiz that developed on the southern fringe of the retreating LIS [*Clark et al.*, 2001]. Drainage of Lake Agassiz eastward through the St. Lawrence River and into the western North Atlantic was originally proposed as the main culprit for the Younger Dryas cooling [*Broecker et al.*, 1989], but the significance of this routing event is jeopardized by the questionable presence of a late Allerød low-salinity signal offshore Nova Scotia [*Keigwin and Jones*, 1995; *de Vernal et al.*, 1996; *Carlson et al.*, 2008b]. A major flooding event through the Mississippi river system is recognized in the Gulf of Mexico, 14.2–14.7 kyr B.P. [*Aharon*, 2006] associated with salinity reductions of 2–4‰ [*Flower et al.*, 2004]. This southern drainage route coincides with MWP 1A and is likely associated with the gradual post-Bølling decrease in AMOC but its timing and geographical position is incongruent with the Younger Dryas cooling. A third freshwater route, directed northward along the McKenzie River and entering the Arctic Ocean has been proposed based on ice sheet modeling [*Tarasov and Peltier*, 2005] and geomorphic evidence [*Murton et al.*, 2010] but compelling paleoceanographic evidence for this event has yet to be produced.

[45] We interpret the major $\delta^{18}O$ depletion peak at the Allerød–Younger Dryas boundary as a signature of meltwater stratification of the upper water mass column (<50–100 m). It is possible that this signal contain a freshwater contribution from the Arctic Ocean brought southward by the East Greenland Current [*Moore*, 2005; *Tarasov and Peltier*, 2005] but this distal source would need to be traced closer to its point of emission. On the other hand, the combined signal of a prominent isotope and IRD peak centered at 13.0–12.8 kyr favor GIS meltwater as a forcing factor for the Younger Dryas cooling.

[46] According to the flooding hypothesis, the Younger Dryas cold reversal is intrinsically linked to the glacial-interglacial transition. This is problematic because although the North Atlantic deglacial progression is modulated by the complex terrestrial runoff from melting ice caps, the sawtooth-shaped structure of the Bølling-Allerød interval implies a mechanism that is common to all D-O cycles. Our analyses highlight a potential interaction between subsurface warm water transports by the Irminger Current and meltwater generated by the former marine-based GIS. Operating independently of LIS flooding scenarios, this mechanism share essential characteristics of the salt oscillator hypothesis originally proposed by *Broecker et al.* [1990] and supports the view that the GIS played a pivotal role in millennial-scale climate cycles [*van Kreveld et al.*, 2000].

6. Conclusions

[47] Our results compared with near-field studies indicate an extended triple-phase deglaciation of the southern GIS as it shrank from its LGM configuration covering the continental shelves to an inland position during early Holocene. Enhanced deposition of ice-rafted tephra from 17.2 kyr B.P. is related to an early deglacial retreat phase on the East Greenland continental margin in vicinity of the Denmark Strait. We infer that breakup of ice shelves in these parts may have begun some 500 years prior to HE 1.

[48] A major recession of the southern GIS during Allerød is inferred from increasing abundances of siliciclastic IRD associated with sharp $\delta^{18}O$ depletions. The trend culminates at ~13 kyr with a discrete depletion peak lasting for more than 400 years across the Allerød–Younger Dryas transition. This Allerød meltwater signal complies with evidence suggesting a rapid glacial unloading of the continental shelves in southern Greenland during the late deglaciation [*Bennike and Björck*, 2002]. The timing and amplitude of this ablation pulse supports a pivotal role for GIS meltwater in the Younger Dryas cooling. A final glacial recession in southern Greenland corresponds to a broad increase in IRD during the early Holocene (9–11 kyr).

[49] We interpret alkenone unsaturation index (UK′37) data from DA04-31P, not as a proxy of local SST, but as reflecting lateral advection of alkenones with the Irminger Current and subsequent subduction in the northern Labrador Sea below the cold East Greenland Current. A comparison with regional ocean climate records points to a generally coherent ISW transport during the Holocene. In contrast, marked variability and digressions in regional SST records are observed throughout the deglaciation. Enhanced ISW transports into the northern Labrador Sea, inferred during the early deglacial, Bølling and Allerød are related to incursions of warm intermediate water masses derived from lower latitudes (e.g., Subpolar Mode Water). Conceivably, the northward penetration of warm subsurface waters are boosted by surface water stratification and limiting vertical mixing imposed by a freshwater cap that formed in the central North Atlantic.

[50] Our analyses, with particular reference to the Bølling-Allerød proxy sequence, points to a linkage between GIS retreat and subsurface ISW transport in the Irminger Current system. Heat exchange between intermediate waters, entering the deep cross-shelf troughs below floating ice shelves is considered as the crucial mechanism for rapid breakup and the consequent release of iceberg armadas. We adhere to earlier held views that ablation products from the melting rims of the GIS was a likely factor for the Younger Dryas cooling. The results call for more high-resolution studies from the southern Greenland margins that can address ice sheet–ocean interactions during submillennial-scale climate cycles. We also stress the value of combining bulk alkenone

analyses with shell-based proxy data as means of elucidating upper ocean dynamics during glacial periods.

[51] **Acknowledgments.** The 2004 cruise of R/V *Dana* organized by the Geological Survey of Denmark and Greenland (GEUS) was financed by the Greenland Bureau of Minerals in Nuuk, Greenland. We gratefully acknowledge the assistance by John Boserup, coring engineer at GEUS, and Ullah Ezat, chemistry engineer at Laboratoire des Sciences du Climat et de l'Environnement Royal NIOZ, Texel, is thanked for performing core logging using the AVATECH XRF scanning instrument. We thank the three anonymous reviewers for constructive assessments of the manuscript. Financial support for various laboratory analyses was provided by the Danish Natural Science Research Council.

References

Aharon, P. (2006), Entrainment of meltwaters in hyperpycnal flows during deglaciation superfloods in the Gulf of Mexico, *Earth Planet. Sci. Lett.*, *241*, 260–270, doi:10.1016/j.epsl.2005.10.034.

Alley, R. B., et al. (2010), History of the Greenland Ice Sheet: Paleoclimatic insights, *Quat. Sci. Rev.*, *29*, 1728–1756, doi:10.1016/j.quascirev.2010.02.007.

Alvarez-Solas, J., S. Charbit, C. Ritz, D. Paillard, G. Ramstein, and C. Dumas (2010), Links between ocean temperature and iceberg discharge during Heinrich events, *Nat. Geosci.*, *3*, 122–126, doi:10.1038/ngeo752.

Andrews, J. T., and K. Tedesco (1992), Detrital carbonate-rich sediments, northwestern Labrador Sea: Implications for ice-sheet dynamics and iceberg rafting (Heinrich) events in the North Atlantic, *Geology*, *20*, 1087–1090, doi:10.1130/0091-7613(1992)020<1087:DCRSNL>2.3.CO;2.

Andrews, J. T., A. E. Jennings, M. Kerwin, M. Kirby, W. Manley, G. H. Miller, G. Bond, and B. Maclean (1995), A Heinrich-like event, H-0 (DC-0), Source(s) for detrital carbonate in the North Atlantic during the Younger Dryas chronozone, *Paleoceanography*, *10*, 943–952, doi:10.1029/95PA01426.

Andrews, J. T., L. M. Smith, R. Preston, T. Cooper, and A. E. Jennings (1997), Spatial and temporal patterns of iceberg rafting (IRD) along the East Greenland margin, ca 68°N, over the last 14 cal ka, *J. Quat. Sci.*, *12*, 1–13, doi:10.1002/(SICI)1099-1417(199701/02)12:1<1::AID-JQS288>3.0.CO;2-T.

Bard, E., B. Hamelin, M. Arnold, L. Montaggioni, G. Cabioch, G. Faure, and F. Rougerie (1996), Deglacial sea-level record from Tahiti corals and the timing of global meltwater discharge, *Nature*, *382*, 241–244, doi:10.1038/382241a0.

Bard, E., M. Arnold, B. Hamelin, N. Tisnerat-Laborde, and G. Cabioch (1998), Radiocarbon calibration by means of mass spectrometric $^{230}Th/^{234}U$ and ^{14}C ages of corals: An updated database including samples from Barbados, Mururoa and Tahiti, *Radiocarbon*, *40*, 1085–1092.

Bendle, J., and A. Rosell-Mele (2004), Distributions of U^{K}_{37} and $U^{K}_{37'}$ in the surface waters and sediments of the Nordic Seas: Implications for paleoceanography, *Geochem. Geophys. Geosyst.*, *5*, Q11013, doi:10.1029/2004GC000741.

Bennike, O., and S. Björck (2002), Chronology of the last recession of the Greenland Ice Sheet, *J. Quat. Sci.*, *17*, 211–219, doi:10.1002/jqs.670.

Bennike, O., S. Björck, and K. Lambeck (2002), Estimates of South Greenland late-glacial ice limits from a new relative sea level curve, *Earth Planet. Sci. Lett.*, *197*, 171–186, doi:10.1016/S0012-821X(02)00478-8.

Björck, S., O. Ingolfsson, H. Haflidason, M. Hallsdottir, and N. J. Anderson (1992), Lake Torfadalsvatn: A high-resolution record of the North Atlantic Ash Zone-I and the last glacial-interglacial environmental changes in Iceland, *Boreas*, *21*, 15–22, doi:10.1111/j.1502-3885.1992.tb00009.x.

Bond, G., W. Broecker, S. Johnsen, J. Macmanus, L. Labeyrie, J. Jouzel, and G. Bonani (1993), Correlations between climate records from North Atlantic sediments and Greenland ice, *Nature*, *365*, 143–147, doi:10.1038/365143a0.

Bondevik, S., J. Mangerud, H. H. Birks, S. Gulliksen, and P. Reimer (2006), Changes in North Atlantic radiocarbon reservoir ages during the Allerød and Younger Dryas, *Science*, *312*, 1514–1517, doi:10.1126/science.1123300.

Broecker, W. S., M. Andree, W. Wolfi, H. Oeschger, G. Bonani, J. Kennett, and D. Peteet (1988), The chronology of the last deglaciation: Implications to the cause of the Younger Dryas event, *Paleoceanography*, *3*, 1–20, doi:10.1029/PA003i001p00001.

Broecker, W. S., J. P. Kennett, B. P. Flower, J. T. Teller, S. Trumbore, G. Bonani, and W. Wolfli (1989), Routing of meltwater from the Laurentide Ice Sheet during the Younger Dryas cold episode, *Nature*, *341*, 318–321, doi:10.1038/341318a0.

Broecker, W. S., G. Bond, M. Klas, G. Bonani, and W. Wolfi (1990), A salt oscillator in the Glacial Atlantic?: 1. The concept, *Paleoceanography*, *5*, 469–477, doi:10.1029/PA005i004p00469.

Carlson, A., J. S. Stoner, J. P. Donnelly, and C. Hillaire-Marcel (2008a), Response of the southern Greenland Ice Sheet during the last two deglaciations, *Geology*, *36*, 359–362, doi:10.1130/G24519A.1.

Carlson, A. E., P. U. Clark, W. R. Peltier, A. De Vernal, and C. Hillaire-Marcel (2008b), Rapid climate change and Arctic Ocean freshening: Comment and reply, *Mem. Geol. Soc. Am.*, *36*, e177–e178.

Cheng, W., and P. B. Rhines (2004), Response of the overturning circulation to high-latitude fresh-water perturbations in the North Atlantic, *Clim. Dyn.*, *22*, 359–372, doi:10.1007/s00382-003-0385-6.

Clark, P. U., S. J. Marshall, G. K. C. Clarke, S. W. Hostetler, J. M. Licciardi, and J. T. Teller (2001), Freshwater forcing of abrupt climate change during the last glaciation, *Science*, *293*, 283–287, doi:10.1126/science.1062517.

Conte, M. H., and G. Eglinton (1993), Alkenone and alkenoate distributions within the euphotic zone of the eastern North Atlantic: Correlation with production temperature, *Deep Sea Res., Part I*, *40*, 1935–1961, doi:10.1016/0967-0637(93)90040-A.

Cuny, J., P. B. Rhines, P. Pearn, and S. Bacon (2002), Labrador sea boundary currents and the fate of the Irminger Sea Water, *J. Phys. Oceanogr.*, *32*, 627–647, doi:10.1175/1520-0485(2002)032<0627:LSBCAT>2.0.CO;2.

Dansgaard, W., et al. (1993), Evidence for instability of past climate from a 250-kyr ice core, *Nature*, *364*, 218–220, doi:10.1038/364218a0.

de Vernal, A., C. Hillaire-Marcel, and G. Bilodeau (1996), Reduced meltwater outflow from the laurentide ice margin during the Younger Dryas, *Nature*, *381*, 774–777, doi:10.1038/381774a0.

de Vernal, A., and C. Hillaire-Marcel (2000), Sea-ice cover, sea-surface salinity and halo-/thermocline structure of the northwest North Atlantic: Modern versus full glacial conditions, *Quat. Sci. Rev.*, *19*, 65–85, doi:10.1016/S0277-3791(99)00055-4.

Denton, G. H., R. B. Alley, G. C. Comer, and W. S. Broecker (2005), The role of seasonality in abrupt climate change, *Quat. Sci. Rev.*, *24*, 1159–1182, doi:10.1016/j.quascirev.2004.12.002.

Dickson, R. R., and J. Brown (1994), The production of North Atlantic Deep Water: Sources, rates and pathways, *J. Geophys. Res.*, *99*, 12,319–12,341, doi:10.1029/94JC00530.

Dowdeswell, J. A., A. Elverhoi, and R. Spielhagen (1998), Glacimarine sedimentary processes and facies on the Polar North Atlantic margins, *Quat. Sci. Rev.*, *17*, 243–272, doi:10.1016/S0277-3791(97)00071-1.

Dowdeswell, J. A., J. Evans, and C. O. Cofaigh (2010), Submarine landforms and shallow acoustic stratigraphy of a 400 km-long fjord-shelf-slope transect, Kangerlussuaq margin, East Greenland, *Quat. Sci. Rev.*, *29*, 3359–3369, doi:10.1016/j.quascirev.2010.06.006.

Elliot, M., L. Labeyrie, G. Bond, E. Cortijo, J. L. Turon, N. Tisnerat, and J. C. Duplessy (1998), Millennial-scale iceberg discharges in the Irminger Basin during the last glacial period: Relationship with the Heinrich events and environmental settings, *Paleoceanography*, *13*, 433–446, doi:10.1029/98PA01792.

Fairbanks, R. G. (1989), A 17,000 year glacio-eustatic sea level record: Influence of glacial melting rates on the Younger Dryas event and deep ocean circulation, *Nature*, *342*, 637–642, doi:10.1038/342637a0.

Fanning, A. F., and A. J. Weaver (1997), Temporal-geographical meltwater influences on the North Atlantic Conveyor: Implications for the Younger Dryas, *Paleoceanography*, *12*, 307–320, doi:10.1029/96PA03726.

Flower, B. P., D. W. Hastings, H. W. Hill, and T. M. Quinn (2004), Phasing of deglacial warming and laurentide ice sheet meltwater in the Gulf of Mexico, *Geology*, *32*, 597–600, doi:10.1130/G20604.1.

Flückiger, J., R. Knutti, and J. W. C. White (2006), Oceanic processes as potential trigger and amplifying mechanisms for Heinrich events, *Paleoceanography*, *21*, PA2014, doi:10.1029/2005PA001204.

Franke, J., A. Paul, and M. Schulz (2008), Modeling variations of marine reservoir ages during the last 45 000 years, *Clim. Past*, *4*, 125–136, doi:10.5194/cp-4-125-2008.

Funder, S., and L. Hansen (1996), The Greenland ice sheet-a model for its culmination and decay during and after the last glacial maximum, *Bull. Geol. Soc. Den.*, *42*, 137–152.

Funder, S., A. E. Jennings, and M. J. Kelly (2004), Middle and late Quaternary glacial limits in Greenland, in *Quaternary Glaciations: Extent and Chronology, Part II*, edited by J. Ehlers and P. L. Gibbard, pp. 425–430, Elsevier, New York.

Gronvold, K., N. Oskarsson, S. J. Johnsen, H. B. Clausen, C. U. Hammer, G. Bond, and E. Bard (1995), Ash layers from Iceland in the Greenland Grip Ice Core correlated with oceanic and land sediments, *Earth Planet. Sci. Lett.*, *135*, 149–155, doi:10.1016/0012-821X(95)00145-3.

Haflidason, H., H. P. Sejrup, D. K. Kristensen, and S. Johnsen (1995), Coupled response of the late Glacial climatic shifts of northwest Europe

reflected in Greenland ice cores - evidence from the northern North Sea, *Geology*, *23*, 1059–1062, doi:10.1130/0091-7613(1995)023<1059:CROTLG>2.3.CO;2.

Hagen, S., and M. Hald (2002), Variation in surface and deep water circulation in the Denmark Strait, North Atlantic, during marine isotope stages 3 and 2, *Paleoceanography*, *17*(4), 1061, doi:10.1029/2001PA000632.

Hanebuth, T., K. Stattegger, and P. M. Grootes (2000), Rapid flooding of the Sunda Shelf: A late-glacial sea-level record, *Science*, *288*, 1033–1035, doi:10.1126/science.288.5468.1033.

Hemming, S. R. (2004), Heinrich events: Massive late Pleistocene detritus layers of the North Atlantic and their global climate imprint, *Rev. Geophys.*, *42*, RG1005, doi:10.1029/2003RG000128.

Hillaire-Marcel, C., A. De Vernal, G. Bilodeau, and G. Wu (1994), Isotope stratigraphy, sedimentation rates, deep circulation and carbonate events in the Labrador Sea during the last ~200 ka, *Can. J. Earth Sci.*, *31*, 63–89, doi:10.1139/e94-007.

Holland, D. M., R. H. Thomas, B. De Young, M. H. Ribergaard, and B. Lyberth (2008), Acceleration of Jakobshavn Isbrae triggered by warm subsurface ocean waters, *Nat. Geosci.*, *1*, 659–664, doi:10.1038/ngeo316.

Hughen, K. A., J. T. Overpeck, S. J. Lehman, M. Kashgarian, J. Southon, L. C. Peterson, R. Alley, and D. M. Sigman (1998), Deglacial changes in ocean circulation from an extended radiocarbon calibration, *Nature*, *391*, 65–68, doi:10.1038/34150.

Hulbe, C. L. (1997), An ice shelf mechanism for Heinrich layer production, *Paleoceanography*, *12*, 711–717, doi:10.1029/97PA02014.

Hulbe, C. L., D. R. MacAyeal, G. H. Denton, J. Kleman, and T. V. Lowell (2004), Catastrophic ice shelf breakup as the source of Heinrich event icebergs, *Paleoceanography*, *19*, PA1004, doi:10.1029/2003PA000890.

Jennings, A. E., K. Gronvold, R. Hilberman, M. Smith, and M. Hald (2002), High-resolution study of Icelandic tephras in the Kangerlussuaq Trough, southeast Greenland, during the last deglaciation, *J. Quat. Sci.*, *17*, 747–757, doi:10.1002/jqs.692.

Jennings, A. E., M. Hald, M. Smith, and J. T. Andrews (2006), Freshwater forcing from the Greenland Ice Sheet during the Younger Dryas: Evidence from southeastern Greenland shelf cores, *Quat. Sci. Rev.*, *25*, 282–298, doi:10.1016/j.quascirev.2005.04.006.

Johannessen, T., E. Jansen, A. Flatøy, and A. C. Ravelo (1994), The relationship between surface water masses, oceanographic fronts and paleoclimatic proxies in surface sediments of Greenland, Iceland, Norwegian Seas, *NATO ASI Ser., Ser. 1*, *17*, 61–85.

Johnson, R. G., and S. E. Lauritzen (1995), Hudson Bay-Hudson Strait jokulhlaups and Heinrich events: A hypothesis, *Palaeogeogr. Palaeoclimatol. Palaeoecol.*, *117*, 123–137, doi:10.1016/0031-0182(94)00120-W.

Johnson, H. L., A. Münchow, K. K. Falkner, and H. Melling (2011), Ocean circulation and properties in Petermann Fjord, Greenland, *J. Geophys. Res.*, *116*, C01003, doi:10.1029/2010JC006519.

Kamb, W. B. (2001), The lubrication basal zone of the West Antarctic ice streams, in *The West Antarctic Ice Sheet: Behavior and Environment*, *Antarct. Res. Ser.*, vol. 77, edited by R. B. Alley and R. A. Bindschadler, pp. 157–199, AGU, Washington, D. C.

Keigwin, L. D., and G. A. Jones (1995), The Marine Record of Deglaciation from the Continental-Margin Off Nova-Scotia, *Paleoceanography*, *10*, 973–985, doi:10.1029/95PA02643.

Knutti, R., J. Flückiger, T. F. Stocker, and A. Timmermann (2004), Strong hemispheric coupling of glacial climate through freshwater discharge and ocean circulation, *Nature*, *430*, 851–856, doi:10.1038/nature02786.

Knutz, P. C., I. R. Hall, R. Zahn, T. L. Rasmussen, A. Kuijpers, M. Moros, and N. J. Shackleton (2002), Multidecadal ocean variability and NW European ice sheet surges during the last deglaciation, *Geochem. Geophys. Geosyst.*, *3*(12), 1077, doi:10.1029/2002GC000351.

Knutz, P. C., R. Zahn, and I. R. Hall (2007), Centennial-scale variability of the British Ice Sheet: Implications for climate forcing and Atlantic meridional overturning circulation during the last deglaciation, *Paleoceanography*, *22*, PA1207, doi:10.1029/2006PA001298.

Kohfeld, K. E., R. G. Fairbanks, S. L. Smith, and I. D. Walsh (1996), *Neogloboquadrina pachyderma* (sinistral coiling) as paleoceanographic tracers in polar oceans: Evidence from northeast water polynya plankton tows, sediment traps, and surface sediments, *Paleoceanography*, *11*, 679–699, doi:10.1029/96PA02617.

Kristjansdottir, G. B., J. S. Stoner, A. E. Jennings, J. T. Andrews, and K. Gronvold (2007), Geochemistry of Holocene cryptotephras from the north Iceland shelf (MD99-2269), Intercalibration with radiocarbon and palaeomagnetic chronostratigraphies, *Holocene*, *17*, 155–176, doi:10.1177/0959683607075829.

Kuijpers, A., S. R. Troelstra, M. A. Prins, K. Linthout, A. Akhmetzhanov, S. Bouryak, M. F. Bachmann, S. Lassen, S. Rasmussen, and J. B. Jensen (2003), Late Quaternary sedimentary processes and ocean circulation changes at the Southeast Greenland margin, *Mar. Geol.*, *195*, 109–129, doi:10.1016/S0025-3227(02)00684-9.

Kvamme, T., J. Mangerud, H. Furnes, and W. F. Ruddiman (1989), Geochemistry of Pleistocene ash zones in cores from the North Atlantic, *Nor. Geol. Tidsskr.*, *69*, 251–272.

Lacasse, C. (2001), Influence of climate variability on the atmospheric transport of Icelandic tephra in the subpolar North Atlantic, *Global Planet. Change*, *29*, 31–55, doi:10.1016/S0921-8181(01)00099-6.

Lackschewitz, K. S., and H. J. Wallrabe-Adams (1997), Composition and origin of volcanic ash zones in Late Quaternary sediments from the Reykjanes Ridge: Evidence for ash fallout and ice-rafting, *Mar. Geol.*, *136*, 209–224, doi:10.1016/S0025-3227(96)00056-4.

Lagerklint, I. M., and J. D. Wright (1999), Late glacial warming prior to Heinrich event 1: The influence of ice rafting and large ice sheets on the timing of initial warming, *Geology*, *27*, 1099–1102, doi:10.1130/0091-7613(1999)027<1099:LGWPTH>2.3.CO;2.

Larsen, L. M., and F. Dalhoff (2006), Composition, age, and geological and geotectonic significance of igneous rocks dredged from the northern Labrador Sea and the Davis Strait, *Rep. 2006/43*, Geol. Surv. of Denmark and Greenland, Copenhagen.

Lavender, K. L., R. E. Davis, and W. B. Owens (2000), Mid-depth recirculation observed in the interior Labrador and Irminger seas by direct velocity measurements, *Nature*, *407*, 66–69, doi:10.1038/35024048.

Lloyd, J. M., L. A. Park, B. Kuijpers, and M. Moros (2005), Early holocene palaeoceanography and deglacial chronology of Disko Bugt, West Greenland, *Quat. Sci. Rev.*, *24*, 1741–1755, doi:10.1016/j.quascirev.2004.07.024.

Long, A. J., D. H. Roberts, M. J. R. Simpson, S. Dawson, G. A. Milne, and P. Huybrechts (2008), Late Weichselian relative sea-level changes and ice sheet history in southeast Greenland, *Earth Planet. Sci. Lett.*, *272*, 8–18, doi:10.1016/j.epsl.2008.03.042.

MacAyeal, D. R. (1993), Binge/purge oscillations of the Laurentide ice sheet as a cause of the North Atlantic's Heinrich events, *Paleoceanography*, *8*, 775–784, doi:10.1029/93PA02200.

Mangerud, J., S. E. Lie, H. Furnes, I. L. Krisiansen, and L. Lomo (1984), A Younger Dryas ash bed in western Norway, and its possible correlations with tephra in cores from the Norwegian Sea and the North Atlantic, *Quat. Res.*, *21*, 85–104, doi:10.1016/0033-5894(84)90092-9.

McCartney, M. S., and L. D. Talley (1982), The sub-polar mode water of the North Atlantic Ocean, *J. Phys. Oceanogr.*, *12*, 1169–1188, doi:10.1175/1520-0485(1982)012<1169:TSMWOT>2.0.CO;2.

Meese, D. A., A. J. Gow, R. B. Alley, G. A. Zielinski, P. M. Grootes, M. Ram, K. C. Taylor, P. A. Mayewski, and J. F. Bolzan (1997), The Greenland Ice Sheet Project 2 depth-age scale: Methods and results, *J. Geophys. Res.*, *102*, 26,411–26,423, doi:10.1029/97JC00269.

Mignot, J., A. Ganopolski, and A. Levermann (2007), Atlantic subsurface temperatures: Response to a shutdown of the overturning circulation and consequences for its recovery, *J. Clim.*, *20*, 4884–4898, doi:10.1175/JCLI4280.1.

Miller, G. H. (2008), Greenland's elusive Younger Dryas, *Quat. Sci. Rev.*, *27*, 2271–2272, doi:10.1016/j.quascirev.2008.10.001.

Moore, T. C. (2005), The Younger Dryas: From whence the fresh water?, *Paleoceanography*, *20*, PA4021, doi:10.1029/2005PA001170.

Moros, M., A. Kuijpers, I. Snowball, S. Lassen, D. Backstrom, F. Gingele, and J. McManus (2002), Were glacial iceberg surges in the North Atlantic triggered by climatic warming?, *Mar. Geol.*, *192*, 393–417, doi:10.1016/S0025-3227(02)00592-3.

Mortensen, A. K., M. Bigler, K. Gronvold, J. P. Steffensen, and S. J. Johnsen (2005), Volcanic ash layers from the Last Glacial Termination in the NGRIP ice core, *J. Quat. Sci.*, *20*, 209–219, doi:10.1002/jqs.908.

Murton, J. B., M. D. Bateman, S. R. Dallimore, J. T. Teller, and Z. R. Yang (2010), Identification of Younger Dryas outburst flood path from Lake Agassiz to the Arctic Ocean, *Nature*, *464*, 740–743, doi:10.1038/nature08954.

Nam, S., R. Stein, H. Grobe, and H. Hubberten (1995), Late Quaternary glacial-interglacial changes in sediment composition at the East Greenland continental margin and their paleoceanographic implications, *Mar. Geol.*, *122*, 243–262, doi:10.1016/0025-3227(94)00070-2.

Ó Cofaigh, C., J. A. Dowdeswell, J. Evans, N. H. Kenyon, J. Taylor, A. Mienert, and M. Wilken (2004), Timing and significance of glacially influenced mass-wasting in the submarine channels of the Greenland Basin, *Mar. Geol.*, *207*, 39–54, doi:10.1016/j.margeo.2004.02.009.

Prahl, F. G., L. A. Muehlhausen, and D. L. Zahnle (1988), Further evaluation of long-chain alkenones as indicators of paleoceanographic conditions, *Geochim. Cosmochim. Acta*, *52*, 2303–2310, doi:10.1016/0016-7037(88)90132-9.

Rahman, A., and A. de Vernal (1994), Surface oceanographic changes in the eastern Labrador Sea: Nannofossil record of the last 31,000 years, *Mar. Geol.*, *121*, 247–263, doi:10.1016/0025-3227(94)90034-5.

Rashid, H., R. Hesse, and D. J. W. Piper (2003), Origin of unusually thick Heinrich layers in ice-proximal regions of the northwest Labrador Sea, *Earth Planet. Sci. Lett.*, *208*, 319–336, doi:10.1016/S0012-821X(03)00030-X.

Rasmussen, T. L., and E. Thomsen (2008), Warm Atlantic surface water inflow to the Nordic seas 34–10 calibrated ka B.P., *Paleoceanography*, *23*, PA1201, doi:10.1029/2007PA001453.

Rasmussen, T. L., D. W. Oppo, E. Thomsen, and S. J. Lehman (2003), Deep sea records from the southeast Labrador Sea: Ocean circulation changes and ice-rafting events during the last 160,000 years, *Paleoceanography*, *18*(1), 1018, doi:10.1029/2001PA000736.

Rasmussen, S. O., et al. (2006), A new Greenland ice core chronology for the last glacial termination, *J. Geophys. Res.*, *111*, D06102, doi:10.1029/2005JD006079.

Reeh, N., M. Christoph, H. Miller, H. Højmark-Thomsen, and A. Weidick (1999), Present and past climate control on fjord glaciations in Greenland: Implications for IRD-deposition in the sea, *Geophys. Res. Lett.*, *26*, 1039–1042, doi:10.1029/1999GL900065.

Rignot, E., M. Koppes, and I. Velicogna (2010), Rapid submarine melting of the calving faces of West Greenland glaciers, *Nat. Geosci.*, *3*, 187–191, doi:10.1038/ngeo765.

Rinterknecht, V., Y. Gorokhovich, J. Schaefer, and M. Caffee (2009), Preliminary ^{10}Be chronology for the last deglaciation of the western margin of the Greenland Ice Sheet, *J. Quat. Sci.*, *24*, 270–278, doi:10.1002/jqs.1226.

Roberts, D. H., A. J. Long, C. Schnabel, S. Freeman, and M. J. R. Simpson (2008), The deglacial history of southeast sector of the Greenland Ice Sheet during the Last Glacial Maximum, *Quat. Sci. Rev.*, *27*, 1505–1516, doi:10.1016/j.quascirev.2008.04.008.

Roberts, D. H., A. J. Long, C. Schnabel, B. J. Davies, S. Xu, M. J. R. Simpson, and P. Huybrechts (2009), Ice sheet extent and early deglacial history of the southwestern sector of the Greenland Ice Sheet, *Quat. Sci. Rev.*, *28*, 2760–2773, doi:10.1016/j.quascirev.2009.07.002.

Ruddiman, W. F., and L. K. Glover (1972), Vertical mixing of ice rafted volcanic ash in North Atlantic sediments, *Geol. Soc. Am. Bull.*, *83*, 2817–2836, doi:10.1130/0016-7606(1972)83[2817:VMOIVA]2.0.CO;2.

Rühlemann, C., and M. Butzin (2006), Alkenone temperature anomalies in the Brazil-Malvinas Confluence area caused by lateral advection of suspended particulate material, *Geochem. Geophys. Geosyst.*, *7*, Q10015, doi:10.1029/2006GC001251.

Shackleton, N. J. (1987), Oxygen isotopes, ice volume and sea level, *Quat. Sci. Rev.*, *6*, 183–190, doi:10.1016/0277-3791(87)90003-5.

Shepherd, A., D. Wingham, and E. Rignot (2004), Warm ocean is eroding West Antarctic Ice Sheet, *Geophys. Res. Lett.*, *31*, L23402, doi:10.1029/2004GL021106.

Sicre, M.-A., Y. Ternois, J.-C. Miquel, and J.-C. Marty (1999), Alkenones in the Mediterranean sea: Interannual variability and vertical transfer, *Geophys. Res. Lett.*, *26*, 1735–1738, doi:10.1029/1999GL900353.

Sicre, M. A., E. Bard, U. Ezat, and F. Rostek (2002), Alkenone distributions in the North Atlantic and Nordic sea surface waters, *Geochem. Geophys. Geosyst.*, *3*(2), 1013, doi:10.1029/2001GC000159.

Sicre, M.-A., L. Labeyrie, U. Ezat, J. Duprat, J.-L. Turon, S. Schmidt, E. Michel, and A. Mazaud (2005), Southern Indian Ocean response to Northern Hemisphere Heinrich events, *Earth Planet. Sci. Lett.*, *240*, 724–731, doi:10.1016/j.epsl.2005.09.032.

Sikes, E. L., J. K. Volkman, L. G. Robertson, and J. J. Pichon (1997), Alkenones and alkenes in surface waters and sediments of the Southern Ocean: Implications for paleotemperature estimation in polar regions, *Geochim. Cosmochim. Acta*, *61*, 1495–1505, doi:10.1016/S0016-7037(97)00017-3.

Simpson, M. J. R., G. A. Milne, P. Huybrechts, and A. J. Long (2009), Calibrating a glaciological model of the Greenland ice sheet from the Last Glacial Maximum to present-day using field observations of relative sea level and ice extent, *Quat. Sci. Rev.*, *28*, 1631–1657, doi:10.1016/j.quascirev.2009.03.004.

Stanford, J. D., E. J. Rohling, S. E. Hunter, A. P. Roberts, S. O. Rasmussen, E. Bard, J. McManus, and R. G. Fairbanks (2006), Timing of meltwater pulse 1a and climate responses to meltwater injections, *Paleoceanography*, *21*, PA4103, doi:10.1029/2006PA001340.

Stein, R., S. Nam, H. Grobe, and H. Hubberten (1996), Late Quaternary glacial history and short-term ice-rafted debris fluctuations along the East Greenland continental margin, in *Late Quaternary Palaeoceanography of the North Atlantic Margins*, edited by J. T. Andrews et al., *Geol. Soc. Sepc. Publ.*, *111*, 135–151.

Stuiver, M., and P. J. Reimer (1993), Extended ^{14}C data-base and revised CALIB 3.0 ^{14}C age calibration program, *Radiocarbon*, *35*, 215–230.

Syvitski, J. P. M., A. B. Stein, J. T. Andrews, and J. D. Milliman (2001), Icebergs and the sea floor of the East Greenland (Kangerlussuaq) continental margin, *Arct. Antarct. Alp. Res.*, *33*, 52–61, doi:10.2307/1552277.

Talley, L. D., and M. S. McCartney (1982), Distribution and circulation of Labrador Sea Water, *J. Phys. Oceanogr.*, *12*, 1189–1205, doi:10.1175/1520-0485(1982)012<1189:DACOLS>2.0.CO;2.

Tarasov, L., and W. R. Peltier (2002), Greenland glacial history and local geodynamic consequences, *Geophys. J. Int.*, *150*, 198–229, doi:10.1046/j.1365-246X.2002.01702.x.

Tarasov, L., and W. R. Peltier (2005), Arctic freshwater forcing of the Younger Dryas cold reversal, *Nature*, *435*, 662–665, doi:10.1038/nature03617.

Thornalley, D. J. R., H. Elderfield, and I. N. McCave (2009), Holocene oscillations in temperature and salinity of the surface subpolar North Atlantic, *Nature*, *457*, 711–714, doi:10.1038/nature07717.

Thornalley, D. J. R., I. N. McCave, and H. Elderfield (2010), Freshwater input and abrupt deglacial climate change in the North Atlantic, *Paleoceanography*, *25*, PA1201, doi:10.1029/2009PA001772.

Ufkes, E., J. H. F. Jansen, and R. R. Schneider (2000), Anomalous occurrences of *Neogloboquadrina pachyderma* (left) in a 420-ky upwelling record from Walvis Ridge (SE Atlantic), *Mar. Micropaleontol.*, *40*, 23–42, doi:10.1016/S0377-8398(00)00030-X.

van Kreveld, S., M. Sarnthein, H. Erlenkeuser, P. Grootes, S. Jung, M. J. Nadeau, U. Pflaumann, and A. Voelker (2000), Potential links between surging ice sheets, circulation changes, and the Dansgaard-Oeschger cycles in the Irminger Sea, 60–18 kyr, *Paleoceanography*, *15*, 425–442, doi:10.1029/1999PA000464.

Veiga-Pires, C. C., and C. Hillaire-Marcel (1999), U and Th isotope constraints on the duration of Heinrich events H0–H4 in the southeastern Labrador Sea, *Paleoceanography*, *14*, 187–199, doi:10.1029/1998PA900003.

Verplanck, E. P., G. L. Farmer, J. Andrews, G. Dunhill, and C. Millo (2009), Provenance of Quaternary glacial and glacimarine sediments along the southeast Greenland margin, *Earth Planet. Sci. Lett.*, *286*, 52–62, doi:10.1016/j.epsl.2009.06.012.

Waelbroeck, C., J. C. Duplessy, E. Michel, L. Labeyrie, D. Paillard, and J. Duprat (2001), The timing of the last deglaciation in North Atlantic climate records, *Nature*, *412*, 724–727, doi:10.1038/35089060.

Wallrabe-Adams, H. J., and K. S. Lackschewitz (2003), Chemical composition, distribution, and origin of silicic volcanic ash layers in the Greenland-Iceland-Norwegian Sea: Explosive volcanism from 10 to 300 ka as recorded in deep-sea sediments, *Mar. Geol.*, *193*, 273–293, doi:10.1016/S0025-3227(02)00661-8.

Wastegård, S., T. L. Rasmussen, A. Kuijpers, T. Nielsen, and T. C. E. van Weering (2006), Composition and origin of ash zones from Marine Isotope Stages 3 and 2 in the North Atlantic, *Quat. Sci. Rev.*, *25*, 2409–2419, doi:10.1016/j.quascirev.2006.03.001.

Weidick, A., M. Kelly, and O. Bennike (2004), Late Quaternary development of the southern sector of the Greenland Ice Sheet, with particular reference to the Qassimiut lobe, *Boreas*, *33*, 284–299, doi:10.1111/j.1502-3885.2004.tb01242.x.

Zahn, R., J. Schonfeld, H. R. Kudrass, M. H. Park, H. Erlenkeuser, and P. Grootes (1997), Thermohaline instability in the North Atlantic during meltwater events: Stable isotope and ice-rafted detritus records from core SO75–26KL, Portuguese margin, *Paleoceanography*, *12*, 696–710, doi:10.1029/97PA00581.

S. Christiansen, Institute for Geography and Geology, University of Copenhagen, Øster Voldgade 10, DK-1350 Copenhagen, Denmark.

H. Ebbesen, P. C. Knutz, and A. Kuijpers, Geological Survey of Denmark and Greenland, Øster Voldgade 10, DK-1350, Copenhagen, Denmark. (pkn@geus.dk)

M.-A. Sicre, Laboratoire des Sciences du Climat et de l'Environnement, IPSL, CNRS/CEA/UVSQ, F-91198 Gif-sur-Yvette, France.